MARMARA UNIVERSITY
INSTITUTE FOR GRADUATE STUDIES
IN PURE AND APPLIED SCIENCES

DESIGN, ANALYSIS AND PRODUCTION OF TEMPERATURE SENSOR USING MICROSTEREOLITHOGRAPHY TECHNIQUE

TAYYAB WAQAR

Ph.D. THESIS

Department of Mechatronics Engineering
Mechatronics Engineering Program

Thesis Supervisor

Prof. Dr. Sezgin ERSOY

ISTANBUL, 2022

MARMARA UNIVERSITY
INSTITUTE FOR GRADUATE STUDIES
IN PURE AND APPLIED SCIENCES

DESIGN, ANALYSIS AND PRODUCTION OF TEMPERATURE SENSOR USING MICROSTEREOLITHOGRAPHY TECHNIQUE

TAYYAB WAQAR
(723516901)

Ph.D. THESIS

Department of Mechatronics Engineering
Mechatronics Engineering Program

Thesis Supervisor

Prof. Dr. Sezgin ERSOY

ISTANBUL, 2022

ACKNOWLEGEMENTS

It is an honour to have more than a couple of people to mention on this page. At first, I would like to thank Allah the almighty for all the strength.

I would like to forward my wholehearted gratitude to my thesis advisor Prof. Dr. Sezgin ERSOY. His constant moral support and trust throughout the research were extremely important.

After that, I would like to offer my gratitude to my wonderful family for all of their prayers, motivation and for being there whenever I need.

"To my loving father, I wish you were still with us. Thank you for everything. I dedicate this and everything to you."

January 2022 **Tayyab WAQAR**

TABLE OF CONTENTS

ÖZET

MİKROSTREOLİTOGRAFİ TEKNİĞİ KULLANILARAK SICAKLIK SENSÖRÜNÜN TASARIMI, ANALİZİ VE ÜRETİMİ

Sensör teknolojilerindeki hızlı gelişmeler, son birkaç on yılda nanoelektronik yapı üretim tekniklerimde yapılan teknolojik ilerlemeden olumlu yönde etkilenmiştir. Mikro fabrikasyon tekniklerinin kullanılması performans ve güvenilirliği artırırken diğer yandan fiziksel boyut, hacim, ağırlık ve maliyetin azaltılmasına da yardımcı olmuştur. 3D baskı teknikleri ve ekipmanları alanındaki sürekli gelişmeler, elektronik yapı, devre ve cihaz imalatı alanında ve diğer birçok alanda kullanılmasını sağlamıştır. Bu ilerleme, silikon bazlı mikro ve hatta nano elektronikler kullanılarak bir entegrasyon yoluyla sensörlerin potansiyel olarak yazdırılmasını mümkün kılmıştır. Halihazırda bu tür cihazların ve yapıların üretimi ve ambalajlanması, ağır bir şekilde yavaş olabilen ve önemli işleme gereksinimleri içerebilen litografiye bağlıdır.

Bu tezin temel amacı, İki Foton Polimerizasyon tabanlı 3B baskı tekniği yöntemlerinden biri olan Doğrudan Lazer Yazı üretim yöntemini kullanarak sıcaklık algılayıcı bir IDT yapısı tasarlamak, analiz etmek ve imal etmektir. Buna ek olarak, geliştirilen algılama yapısının Sonlu Elemanlar Analizi ve modellenmesi ve sıcaklıktaki değişimler kullanılarak karakterizasyonu bu çalışmanın en önemli amaçları arasındadır.

Yüzey akustik dalgası kullanılarak sıcaklık algılamanın çalışma prensibi detaylı olarak araştırılmış ve son imalat sürecinden önce algılama yapısının tasarımını optimize etmek için sonlu eleman tabanlı çalışmalar yapılmıştır. Simülasyon yoluyla elde edilen sonuçlar ışığında IDT yapıları üretilmiştir. Üretilen yapılar daha sonra üretim sırasında herhangi bir kusur olup olmadığını kontrol etmek için elektron mikroskobu kullanılarak incelendi. Daha sonra, bir vektör ağ analizörü kullanılarak rezonans frekans tepkileri ölçüldü. Buna ek olarak, fabrikasyon algılama yapılarının karakterizasyonu gerçekleştirilmiştir. Son olarak, bu çalışmanın ön sonuçları sunulmuş ve simülasyon ve pratik testler ile karşılaştırması yapılmıştır.

Ocak 2022 **Tayyab WAQAR**

ABSTRACT

DESIGN, ANALYSIS AND PRODUCTION OF TEMPERATURE SENSOR USING MICROSTEREOLITHOGRAPHY TECHNIQUE

The rapid advancements in sensor technologies have been affected positively by the technological progress that has been made my nanoelectronics structure fabrication techniques over the last few decades. The use of micro-fabrication techniques has increased the performance and reliability, while on the other hand, it has also helped in reducing the physical size, volume, weight, and cost. Continuous developments in the field of 3D printing techniques and equipments have enabled its usage in the field of electronics structures, circuits, and devices fabrication as well beside many other fields. This advancement has enabled the potential printing of sensors, via integration using silicon-based micro or even nanoelectronics. Currently, the manufacturing and packaging of such devices and structures are heavily reliant on lithography, which can be slow and can involve substantial processing requirements.

The main aim of this thesis is to design, analyze and fabricate a temperature sensing IDT structure by employing the Direct Laser Writing fabrication method which is one of the forms of Two-Photon Polymerization based 3D printing technique methods. In addition to that, Finite Element Analysis and modeling of the developed sensing structure and the characterization using changes in temperature are among the most important objectives of this study.

The working principle of temperature sensing using surface acoustic wave was researched in detail and finite element-based studies were performed to optimize the design of the sensing structure before the final fabrication process. In the light of the results obtained through simulation, the IDT structures were fabricated. The fabricated structures were then inspected using an electron microscope to check for any defects during the fabrication. Afterward, their resonant frequency response was measured using a vector network analyzer. In addition, the characterization of the fabricated sensing structures was performed. Finally, the preliminary results of this study are presented and the comparison with the simulation and practical testing is performed.

January 2022 **Tayyab WAQAR**

CLAIM FOR ORIGINALITY

Temperature sensing IDT structures, in micrometer dimensions, were modelled, analyzed and fabricated using Direct Laser Write based 3D printing technique in this research. At present, the fabrication of such structures and sensors is normally realized using conventional lithography techniques. These conventional fabrication methods require strict following of the processes in order to produce the exact same results and hence are more time consuming. The proposed method is based on using a 3D printer to realize the fabrication of the sensor and is automated, therefore, it requires comparatively much less effort and time. The novelties of this research are stated below:

- Two-Photon Polymerization based Direct Laser Writing technique was utilized for the fabrication of the sensing IDT structure using a 3D printer. 3D printers are normally employed for printing macro size structures. Many printing techniques that can utilized for the production of structures in micro sizes have been researched and a couple of printers are produced in recent years. However, the novelty of this study is to employ such printer to fabricate a temperature sensing IDT structure using a mixture of Gold and Chromium materials with the smallest feature size as little as 3 μm. The originality of this research lies in the production of such a structure a 3D printer with low cost and very little workload. Nothing similar to our research was observed during the literature review.

January 2022 **Assoc. Prof. Dr. Sezgin ERSOY** **Tayyab WAQAR**

LIST OF PUBLICATIONS

- *"Surface Acoustic Wave Sensing",* Encyclopedia of Sensors and Biosensors (Elsevier). (Accepted, To be published in 1st quarter of 2022).
- *"Manufacturing of Microfluidic Sensors Utilizing 3D Printing Technologies: A Production System",* Journal of Nanomaterials, Online Link. (Published in August 2021)
- *"Design and Analysis Comparison of Surface Acoustic Wave-Based Sensors for Fabrication Using Additive Manufacturing",* Journal of Nanomaterials, Online Link. (Published in July 2021)
- *"Fabrication of Bidirectional Electrothermal Microactuator by Two-Photon Polymerization",* Current Nanoscience, Online Link (Accepted for Publication, October 2020).
- *"Direction-Action Research for Design, Analysis, and Fabrication of Temperature Sensor Using Microstreolitography Technique",* Online Link (Published in October 2019).

SYMBOLS

$\mathbf{Q}$	: Quality Factor
$\boldsymbol{T_p}$	: Stress (Pa)
$\boldsymbol{S_q}$	: Strain
$\boldsymbol{E_k}$	: Applied Electric Field (volt/m)
$\boldsymbol{c_{pq}^E}$	: Stiffness (Pa)
$\boldsymbol{D_i}$	: Electric displacement (coulomb/m^2)
$\boldsymbol{e_{iq}}$	: Dielectric tensor of the material
$\boldsymbol{\varepsilon_{ik}^S}$	: Permittivity constant
$\boldsymbol{k^2}$	: Electromechanical coupling factor
$\boldsymbol{v_R}$	: Velocity of Rayleigh Wave (m/s^2)
$\boldsymbol{v_S}$	: Velocity of Shear Wave (m/s^2)
$\boldsymbol{v}$	: Poisson's ratio
$\boldsymbol{\mu}$	: Shear modulus (N/m^2)
$\boldsymbol{\rho}$	: Density (g/cm^3)
$\boldsymbol{E}$	: Elastic modulus
$\boldsymbol{\lambda}$	: Wavelength (nm)
$\boldsymbol{P_L}$	: Period Length
$\boldsymbol{f_0}$	: Center Frequency of resonator (MHz)
$\boldsymbol{\eta}$	: Metallisation Ratio
$\boldsymbol{\tau}$	: Delay Time (ms)
$\boldsymbol{S_{21}}$	: Transmitting parameter (dB)

P_{out} : Output power (dB)

P_{in} : Input power (dB)

S_{11} : Input reflection of the signal (dB)

S_{12} : Reverse transmission (dB)

S_{22} : Output reflection of the signal (dB)

a_n : Incident wave

b_n : Reflected wave

Δf : Bandwidth of the resonator (nm)

N_p : Number of input IDT electrode pairs

ε : Relative Permittivity (F/m)

C : Coupling Matrix (C/m^2)

ABBREVIATIONS

2PP	: Two-Photon Polymerization
AJ	: Aerosol Jet
CAD	: Computer Aided Design
DiLL	: Dip-in Laser Lithography
DLW	: Direct Laser Write
DUT	: Device Under Test
FEA	: Finite Element Analysis
IDT	: Interdigital Transducers
IL	: Insertion Loss
MEMS	: Micro Electro-Mechanical Systems
NDT	: Non-Destructive Testing
NEMS	: Nano Electro-Mechanical Systems
NIR	: Near-Infrared
Q	: Quality Factor
RFID	: Radio Frequency Identification
SAW	: Surface Acoustic Wave
SEM	: Scanning Electron Microscopy

LIST OF FIGURES

LIST OF TABLES

1. INTRODUCTION

The aim of this chapter is to introduce the motivation and objectives of this research. In addition to that, this chapter also provides introduction to Surface Acoustic Wave (SAW) sensors along with their history, working principle and applications. This chapter also covers the topics of fabrication of sensor using 3D printing technique especially for SAW sensors. Organization of the thesis is also provided in this chapter.

1.1 Aim and Objectives:

Sensors have become an integral part of our everyday lives by helping us converting packets of data to make important decisions. Due to this reason, researches are done constantly to improve the fabrication processes of sensors by making them more user-friendly, less time-consuming, and more cost-effective. The application of any fabrication solution that offers those advantages will have a major impact on the manufacturing of modern sensors. In order to address this, a Micro Electro-Mechanical Systems (MEMS) based 3D printed SAW structure for the detection of temperature has been presented in this thesis. To realize the fabrication of the said SAW structure, initially the designing and analysis, Finite Element Analysis (FEA), were performed using computer simulation software such as COMSOL. Optimal conditions were examined and deduced in the virtual domain before moving on with the fabrication of the structure. To summarize, the objectives of this thesis are:

- Designing of a SAW structure
- Analysis of the designed SAW Interdigital Transducers (IDT) structure using computer simulation program such as COMSOL
- Investigation for the possibility of 3D printing the designed and analysed SAW IDT structure
- Fabrication of SAW IDT structure using 3D printing techniques
- Characterization of the fabricated IDT structures

1.2 Overview:

Sensor-based technologies are playing an enormous role in fostering social and economics-based advancements in emerging economies all over the globe. To support the

necessary technological development in the field of printed electronics [1–3] , hence in the field of sensors, both the researchers [4] and the industries [5] are working in alignment. Research and development are done to cut down the costs [6] and the time [7] to mass-produce sensors that are directly related to the efficiency [8–10] of the production and carries a huge benefit for the industry and also to the end-user. One such technique which can help the advancements towards this common goal is known as 3D printing and it is already being employed to produce parts for industries such as automotive which greater speed and accuracy. To facilitate the process of 3D printing for sensor manufacturing, ink-jet printing, a technology commonly used in both personal and commercial environments, has surfaced in preference to conventional electronics fabrication practices [11–14]. Au Et al. compared the cost of a traditionally manufactured sensor, i.e. via lithography, to a 3D printed technology, i.e. stereolithography, and found the difference to be 15 USD [15]. Not only the cost, but the simplicity of the 3D printing technique plays an important role here as it makes the reproduction of the same structure with minimal human effort. In addition to that, the sensitivity, and the accuracy of the printed sensor, compared to the traditional ways, are not affected [16, 17].

Several 3D printing technologies are being currently utilized and are also researched for their implementation in the sensor fabrication process and one of them is based on Aerosol Jet (AJ) method which can directly print the required sensing structure on the provided substrate. AJ-based direct structure writing technique has been used for the realization of strain sensor [18–20], electrochemical and biosensors [21], antennas [22], electronic interconnect devices [23], transistors [24], solar cells [25, 26], electrothermal actuators [27] and microbeams [28]. This works focuses on the use of the AJ-based printing method for the Surface Acoustic Wave (SAW) based passive temperature sensor.

SAW devices have found variety of applications in fields ranging from harsh environmental monitoring systems to communication systems and so on. They are majorly being deployed as filters, oscillator and sensors too. Their theory was first put forward by Lord Rayleigh in 1885 [29]. SAW-based devices use the principle of piezoelectric effect to convert an electrical signal to a mechanical wave, Rayleigh wave which is a transversal wave, which then propagates through the piezoelectric substrate to the other transducer which then changes it back to an electric signal. The properties of the

Rayleigh wave and the principle of the piezoelectric effect need to be understood correctly for the application of them as a sensing device [30].

A radio wave is emitted using a wireless interrogation device which then energizes the SAW device using the opposite of the piezoelectric effect. The radio wave is transferred to IDT via an antenna. The IDT converts the received electrical signal to a transversal wave, Rayleigh wave, which then propagates along the piezoelectric substrate to form a resonator. This structure has a unique resonating frequency at each temperature and once the structural parameters of the SAW resonator are known, it can be utilized as a temperature sensing structure [31].

SAW sensors first gained attention in 1960s due the rise of Non-Destructive Testing (NDT) of systems where researchers thought that they could play an integral role in the experimentation and testing. The idea was supported by many publications which investigates the theoretical process of generating surface acoustic waves [32]. Depending on that, the very first SAW sensor, in the form of a uniform IDT produced on a crystal quartz substrate, was fabricated in 1965 [33]. That accelerated the researches in SAW device in the form of suitable piezoelectric materials to be deployed as substrate [34–36] and also regarding the fabrication technology for the production of such devices. These studies concluded that the accuracy of SAW devices is directly dependent on its frequency and the dimensions of IDT. In the light of these conclusions, millions of SAW devices are produced and used for multitude of applications.

Due to the small dimensions, low cost, and great sensitivity of SAW sensors, they are currently favoured over the other sensors. These devices can measure many physical factors i.e., temperature, pressure, gas and humidity. Some of the most distinct features of the SAW devices are their ability to be deployed in harsh environments and their ability to work in a passive wireless manner. In 1980s, after the results of studies related to SAW sensors were published, their potential applications in several fields started to appear.

One of the early studies into SAW sensing resulted in the modelling of their equivalent circuit in 1960s [37]. This research formed the foundations of a later study which developed a delta function model of SAW device in 1970s [38]. Taking advantage of those results, an impulse response model of the SAW device was developed in 1970s

[39]. These early researches formed the foundations for the current studies to be conducted in the field of SAW that focuses more on performance improvements. In the late 1970s the variables related to the electrical and mechanical properties of SAW in the form of mixed matrix SAW transducer was described [40]. Application of coupling of modes model, most popular method for modelling SAW currently and initially utilized for microwave modelling, was performed in the late 1980s [41]. This model was then further developed in early 2000s ultimately transforming the P-matrix to transmission matrix hence forming the basis of application of cascaded SAW devices [42].

With the advances in computing technology, several tools for FEA were developed which produces much more accurate analysis results for SAW devices with complex structures in terms of both geometry and materials. Examples of these tools includes COMSOL and ANSYS among others. These tools are utilized for the simulation of delay line configuration [43], dimension reduction of SAW model [44], high frequency modelling of SAW devices [45], and modelling of wireless SAW systems [46] among other different parameters. In addition to above mentioned FEA approaches, many commercially targeted applications of SAW devices have also been developed. A couple of example includes a passive wireless sensor using USRP B200mini [47] and a university fabricated SAW device which utilizes orthogonal frequency coding technique [48]. Fabricated SAW devices are also used to detect and measure temperature [49], pressure [50], strain in process monitoring [51], torque monitoring [52], chemical vapours and gases [53] and biosensing applications [54].

SAW-based sensors can provide medical [55], telecommunication [56], consumer electronics [57, 58], automotive [55] and industrial [57] sectors with a wide range of use cases. Due to their passive sensing capabilities, SAW devices can be utilized in harsh operating conditions where normal electronic circuits cannot be used i.e. high temperatures. Normally, SAW-based sensors are fabricated using traditional methods which requires a clean room facility and the obligation to follow complicated several step processes [59] using lithography [60] but the advancements in the 3D printing technologies have allowed the researchers to apply them to sensor fabrication process. These technologies can directly print nanoparticles onto the substrate to fabricate a

sensing structure. They decrease the process steps and allows the efficient use of the materials as compared to traditional lithography [61–64].

For this work, the AJ-based stereolithography printing method will be of the focus. This printing method will be explored for the fabrication of a SAW-based temperature sensor. The development of such a sensor is very much in line with the current requirements of many industries. [65–69].

1.3 Organization of Thesis:

This dissertation is organized into 5 separate section. All of these sections provide the necessary explanation to understand the aim, theory, workflow process and results of this research. Those sections are:

- Introduction
- SAW Sensing: Introduction, Theory and Devices
- Design and Fabrication Methodology
- Results and Discussion
- Conclusions

The introduction defines the motivation and objectives of this research. In addition to that, this chapter also provides literature review, introduction to SAW sensors along with their history, working principle and applications. This chapter also covers the topics of fabrication of sensor using 3D printing technique especially for SAW sensors. Organization of the thesis is also provided in this chapter.

The theory behind the working of the SAW sensor, piezoelectricity, is described in the 2nd chapter. This is very much a requirement for anyone in order to grasp the working principle of the SAW sensing. In addition to that material properties for SAW sensing, Rayleigh waves and devices based on Rayleigh wave are described in this section. Finally, different types of SAW resonators, their important parameters and characteristics, and the application of SAW for the measurement of different physical quantities are also described in this chapter.

In chapter 3, the design parameters of the proposed IDT structures are described. The governing equations for those parameters are also presented in this chapter. Afterward,

introduction and a brief literature review of the proposed DLW based on 2PP 3D printing technique is presented. The workflow process using this technique for the fabrication of the IDT structure is illustrated. Finally, the Computer Aided Design (CAD) of the IDT structures using the computer software is presented in this section.

Chapter 4 presents the results of the fabrication of the proposed IDT structures. Electron microscope images of the IDT structures are presented in this section. Afterwards, the results of the simulation studies are presented. In addition to that resonant response of the IDT structures are provided. Finally, the temperature response of the IDT structures is presented in this chapter.

The conclusion for the whole dissertation is provided in the final chapter. Comparison of the simulated and experimental analysis is done in this section. Finally, the dissertation is completed by provided the recommendation for the future research.

2 SAW SENSING: INTRODUCTION, THEORY AND DEVICES

All SAW devices utilize the piezoelectric effect for converting an electrical signal to a mechanical wave using IDTs fabricated on a piezoelectric substrate and vice versa. The generated waves are transversal waves in nature and are known as Rayleigh waves.

2.1 Piezoelectricity:

The piezoelectric effect, discovered in 1880 by Paul and Pierre [70], describes a phenomenon where an application of electrical voltage results in mechanical strain in piezoelectric materials. The reverse of this effect was also demonstrated a little while later where the application of mechanical stress on piezoelectric materials resulted in the generation of electric potential. Hence, such materials can be implemented as actuators [71]. This phenomenon is shown in figure 2.1.

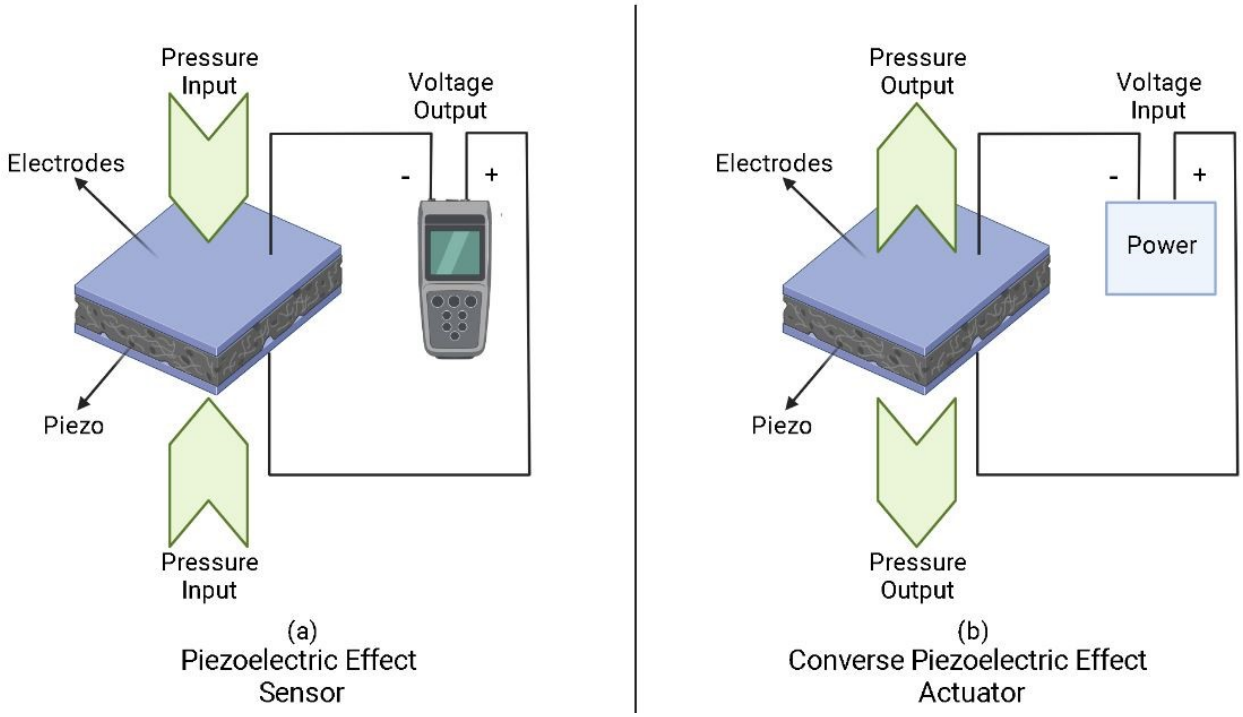

Figure 2.1. Working principle of (a) Piezoelectric Effect and (b) Converse Piezoelectric Effect.

After the modelling of this phenomenon [72] practical applications of the piezoelectric effects in the form oscillators started to surface [73]. Researchers started to look into the materials that are more suited to piezoelectric effect for clearly defined implementations [74] and parallel to the developments in material sciences piezo-based transducer and

filters for the specific applications started to appear [75]. To date researches are being actively done in this field for implementation of piezo based materials as sensors [76] and actuators [77].

It can be observed from the figure 2.1 the piezoelectric effect is the result of the change in electrical charges due to the application of pressure, i.e. mechanical strain. This resulting deformation in the material [78] due to the application of mechanical strain cause the occurrence of voltage. The converse piezoelectric effect happens when the applied voltage on such a material [79] cause a deformation in it. This mechanical strain in piezoelectric materials can be described by the following equation [80].

$$T_p = c_{pq}^E S_q - e_{pk} E_k \tag{2.1}$$

Where:

T_p = Stress (Pa)

S_q = Strain

E_k = Applied Electric Field (volt/m)

c_{pq}^E= Stiffness (Pa), where E represent stiffness measured at constant electric field

$$D_i = e_{iq} S_q - \varepsilon_{ik}^S E_k \tag{2.2}$$

Where:

D_i = Electric displacement (coulomb/m^2)

e_{iq}= Dielectric tensor of the material

ε_{ik}^S= Permittivity constant, where S represent values measured at constant strain

The conversion rate between the electrical and mechanical energy is defined by the electromechanical coupling factor, k^2, of the utilized material. It is can be expressed as [81]:

$$k_{ij}^2 = \frac{d_{ij}^2}{\varepsilon_{ii}^S S_{jj}^E} \tag{2.3}$$

2.2 Poling and Piezoelectric Materials:

Piezoelectric materials are capable of observing piezoelectric effect, once pressure or electrical load is applied, after undergoing an artificial poling process. The whole poling process is depicted in figure 2.2. Most of the piezoelectric materials have their dipoles randomly aligned as shown in figure 2.2(a). In order to increase the piezoelectric effect capability of those materials poling process is performed. During the poling process, the material is left under an electric field below its Curie temperature hence aligning its poles in one single direction, figure 2.2(b). Once the electric field is removed, the majority of the poles stays aligned in the same direction figure 2.2(c). The ability of these materials to keep their dipoles aligned in the same direction after the removal of the electrical field is known as ferroelectricity.

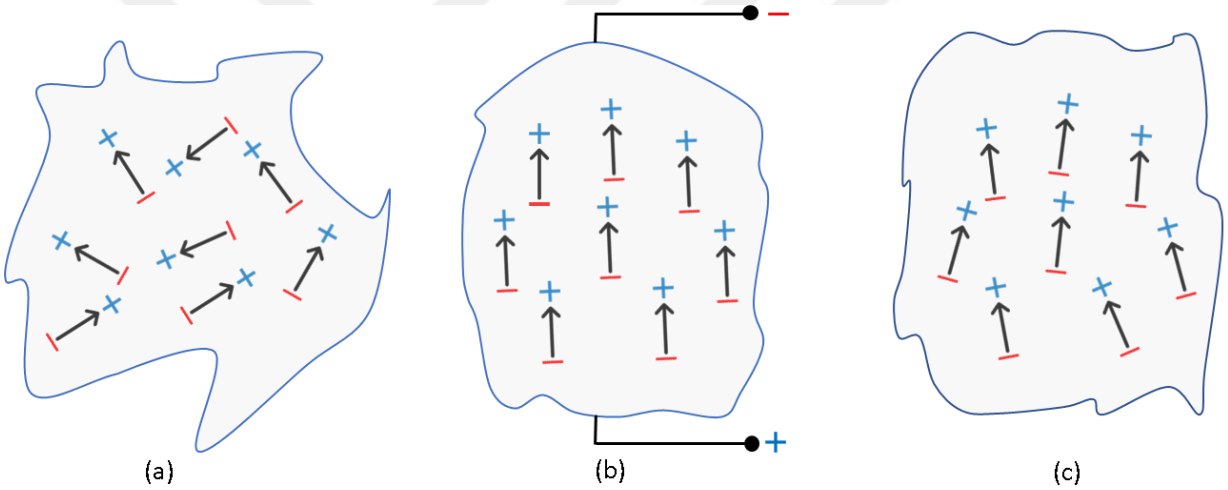

Figure 2.2. Material poling process (a) unpoled material, (b) material during the poling process, (c) poled material.

Piezoelectric effect is applied in many industrial applications [82] ranging from consumers electronic devices [83] such as buzzers, speakers, input devices [84] to medical and communication devices as ultrasonic devices [85] and filters. Some examples are:

- To sense pressure, strain in the form of mechanical sensors [86]
- To convert mechanical energy to electrical energy in energy harvesters [87]
- Lighters

2.3 Surface Acoustic Waves:

2.3.1 Rayleigh waves:

SAW was first discovered in 1885 by Lord Rayleigh and was proposed in his paper [29]. SAW is widely used to describe many different types of waves[88] that propagate close to the material surface. Medium of propagation, layers of propagation and boundary conditions are some of the parameters [89, 90] which determine the type of wave among many different existing waves. Rayleigh wave is among those wide variety of SAW [91] and it is one of the most common mode of operation for SAW device. The depiction of Rayleigh SAW is presented in figure 2.3. These waves occur close to material's surface while depicting its particle having elliptical motion perpendicular to the direction of propagation [92]. The amplitude of these waves appears to decrease along the depth of the material [93].

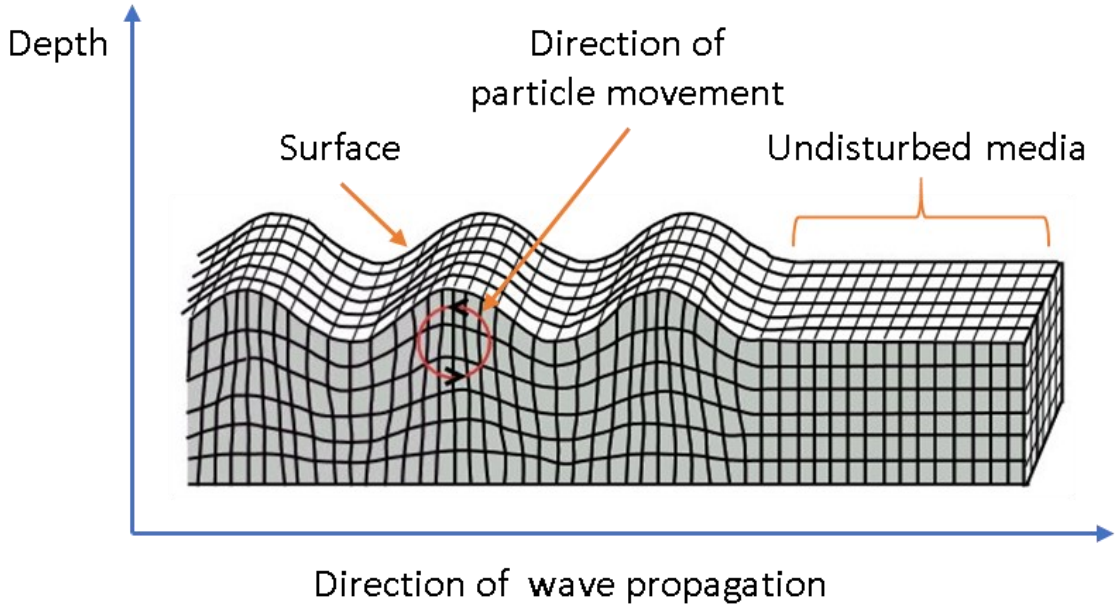

Figure 2.3. Representation of SAW, in the form of Rayleigh wave, showing particle motion and wave propagation.[94]

2.3.2 Velocity of Rayleigh Waves:

Finding the velocity (v) of the SAW in a substrate material for the specific direction of propagation is one of the important parameters for it to be utilized as a sensor. The properties of substrate material are used for the determination of Rayleigh waves velocity.

Substrate material properties can be approximated using set of equation of motion in a piezoelectric setting[95]. Details of this method, which was initially suggested in 1968 [96], are presented by Slobodnik et al. in 1973 [97].

The velocity of Rayleigh waves is directly related to the substrate material's density and its elastic moduli [98]. In 1998, a formula to estimate the velocity of Rayleigh waves was presented by Freund [99]:

$$v_R = v_S \frac{0.862 + 1.14\upsilon}{1 + \upsilon} \tag{2.4}$$

Where:

v_R = Velocity of Rayleigh Wave

v_S = Velocity of Shear Wave

υ = Poisson's ratio

Shear wave velocity can be defined as the ratio of shear modulus (μ) to density (ρ) [100] and can be expressed as:

$$v_S = \sqrt{\frac{\mu}{\rho}} \tag{2.5}$$

Shear modulus is also represented by G sometimes. Shear modulus (μ) can be defined as the ratio of elastic modulus (E) and Poisson's ratio (υ):

$$\mu = \frac{E}{2(1 + \upsilon)} \tag{2.6}$$

The energy of Rayleigh waves is at its maximum due to the nature of their propagation [101]. Since the Rayleigh waves appear on the surface of substrate material a decrease in their energy profile is noticed with the increase in substrate depth [102]. This decrease is approximately denoted as:

$$e^{-2\pi\frac{y}{\lambda}} \tag{2.7}$$

Where:

y = Distance from the surface of substrate material

λ = Wavelength

2.4 Components of SAW Sensor

The components of SAW devices change according to its type, but all of those SAW devices have two most important components.

- Interdigital Transducer (IDT)
- Reflector Grating Patterns

These two basic components of SAW devices are used for signal (wave) generation, transducing action and processing of the generated wave.

2.4.1 Interdigital Transducer (IDT) Parameters

IDTs are arguably the most important part of any SAW device as their main job is to convert the collected electric signals to surface waves and vice versa using the piezoelectric properties of the substrate material. IDTs are basically a collection of strips developed using any conductive material on top of a piezoelectric suitable substrate. They can be deployed in many different patterns [93], i.e. single electrode and double electrode IDT configuration among others.

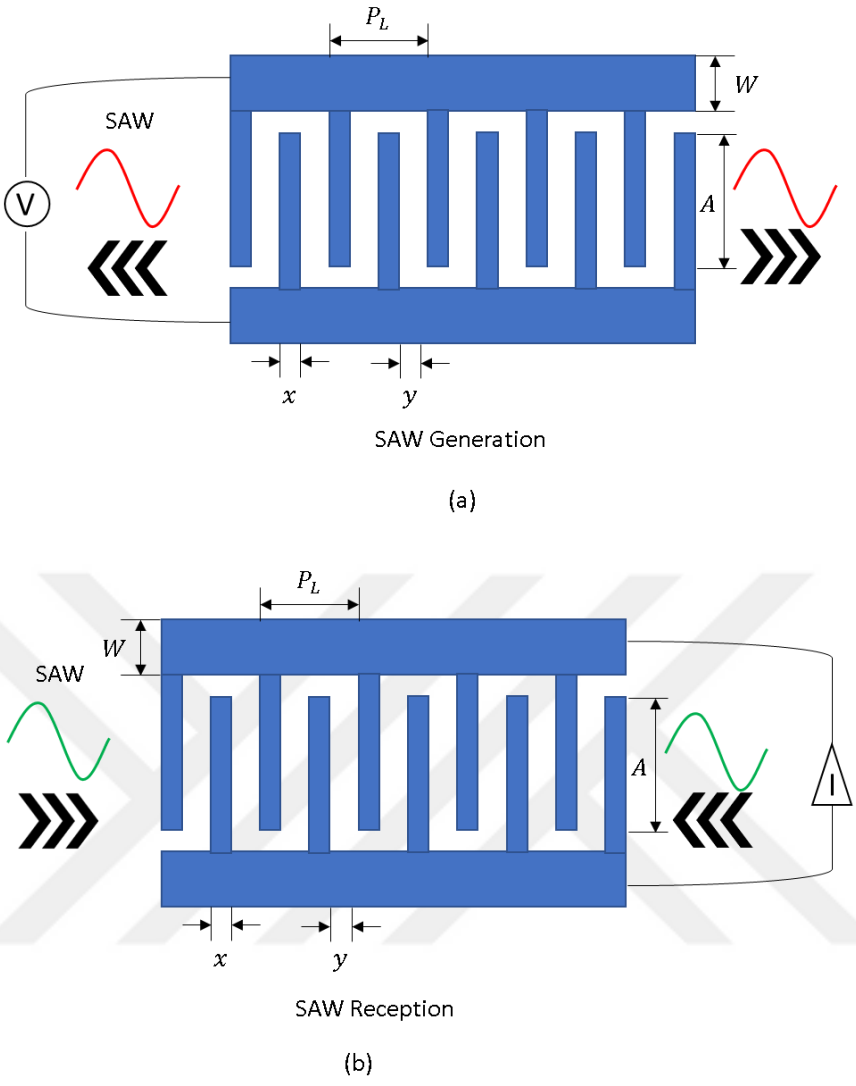

Figure 2.4. Structure illustration of a single electrode SAW IDT with its parameters (a) wave generation and (b) wave reception. [103, 104]

The basic structure of a single electrode type SAW IDT, along with its parameter, is illustrated in Figure 2.5 [90]. Figure 2.5(a) illustrates the function of a SAW device in SAW generating mode. In this mode, a voltage potential between busbars causes the substrate to contract and expand under the converser piezoelectric effect. This simultaneously contracting and expansion of substrate due to the changing electric field between electrode fingers results in the formation of SAW in both directions. The working of SAW device in reception mode is shown in figure 2.5(b). This mode utilizes the piezoelectric effect to convert the SAW, mechanical waves, to current. Thus, using these properties of SAW device, it can be utilized as signal processing applications.

Most of the basic parameters of a SAW based device, such as bandwidth, center frequency etc., are directly related to the design of its IDT structure. Hence, the designing of IDT becomes a very crucial part of any SAW device. Mainly, the period length (P_L) of the generated SAW is equal to its wavelength (λ). Both of these parameters are calculated depending on the velocity of SAW (v_R) and its center frequency (f_0) as shown in equation 2.8.

$$P_L = \frac{\lambda}{v_R} = \frac{1}{f_0} \tag{2.8}$$

In figure 2.5, x and y represent width of IDT electrode and distance between two electrode fingers respectively. The length of period, for IDT shown in figure 2.5, can be calculated using:

$$P_L = 2 \times (x + y) \tag{2.9}$$

This design utilizes the most common value, 0.5, for metallisation ratio (η). This can be calculated as:

$$\eta = \frac{x}{x + y} \tag{2.10}$$

The metallisation ratio of 0.5 means that the width of electrode finger and the gap between electrode finger is of same length. The delta model-based simulation method, showing how the device operates, has been developed [38].

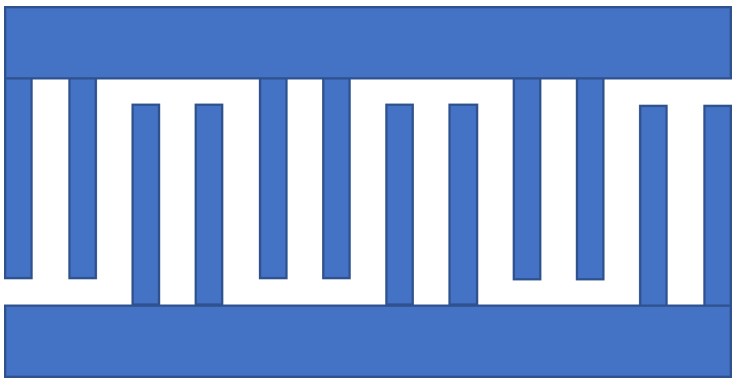

Figure 2.5. Structure illustration of a double electrode SAW IDT

Many different configurations for electrodes have been proposed for SAW device due to their importance. A double electrode-based IDT configuration is shown in figure 2.6 [105].Other forms of IDTs that are proposed includes apodised structure based IDTs [38], multiple electrodes based multi finger IDTs [88],unidirectional IDTs [106] and many others [107]. Impedance matching of network must be something that needs to be taken into consideration while deciding on IDT structures [108].

2.4.2 Reflector Gratings

The main purpose of reflector gratings in a SAW device is to increase the in-phase reflection of the incident SAW. Several different types of reflective gratings that are commonly utilized in SAW devices are presented in figure 2.7. These gratings can be in hundreds in relation to the requirement of the application for SAW device.

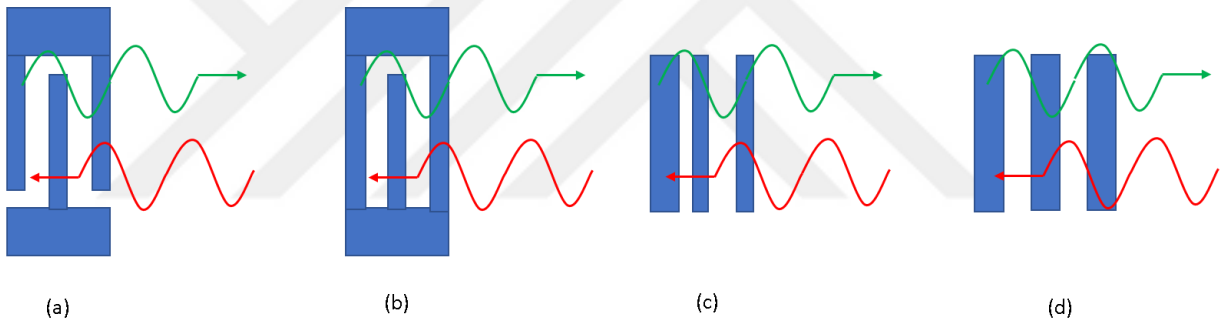

Figure 2.6. Different types of reflector grating configurations (a) IDT type (b) shorted IDT type (c) open type (d) bar type.[109]

Many other different configurations for reflective grating for SAW are also researched [110]. Majority of SAW devices implemented today utilizes line-based electrode gratings as reflective grating still there are some researches for dot based reflective gratings [111].

2.5 Configuration of SAW Devices

Since 1965, when SAW was first introduced [33], it has been implemented in many different application areas utilizing different configurations. The leading industry for SAW device is communication, deploying millions of SAW devices every year, where this technology has been implemented in the form of filters and oscillators using delay line configuration [88]. SAW based filters and oscillators are preferred in industrial

application because of their capability to work under extreme conditions, a single chip solution for filtering, stability and low cost [112]. Many different configurations of SAW devices can be developed using the components of SAW, defined above, in different combinations. Delay line and resonator-based configuration of SAW devices are the two mostly used configurations of SAW.

2.5.1 Resonator

SAW based resonators are devices that have reflective gratings formations on either side of IDT or IDTs in order to confine the SAW energy inside the resonant cavity. They were first proposed in 1970 [113] with different configurations of them presented later on [114]. Resonators can be employed for controlling frequency in oscillators, for filtering in communication system and also as sensors [115]. There are wide variety of SAW based resonator structures [115] with two main configurations for SAW based resonator structure described below.

2.5.2 One-port SAW resonator

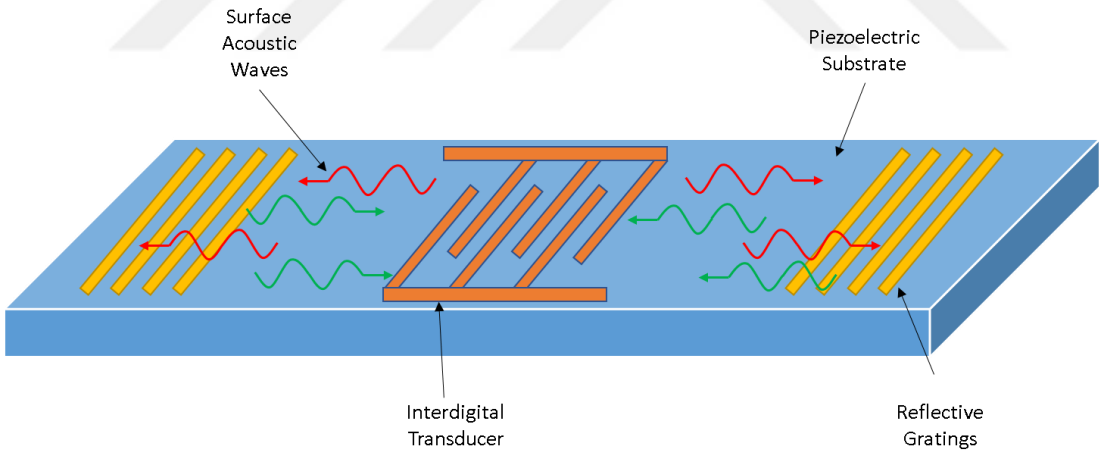

Figure 2.7. Single-port SAW resonator structure.

Schematic of a typical one-port SAW resonator is illustrated in figure 2.8. This type of configuration has an IDT structure fabricated on top of a piezoelectric substrate with reflective grating structures on either side of IDT structure. In this configuration, a single IDT is utilized for input and as well as output of the signal. Acoustic aperture of the device, number of electrode pairs in IDT, number of reflectors grating and spacing between them are some of the important parameters for a single-port resonator.

2.5.3 Two-port SAW resonator

A typical double port SAW based resonator is shown in figure 2.9. The majority of the structure is similar to a single-port resonator with the exception of a pair of IDTs. One of the IDTs is used for input and the other one is utilized for output of the signal. In addition to the parameters described above for single-port resonator, the distance between the reflective gratings and IDTs and substrate properties are some of the important parameters that should be considered while designing a two-port resonator device. [88]

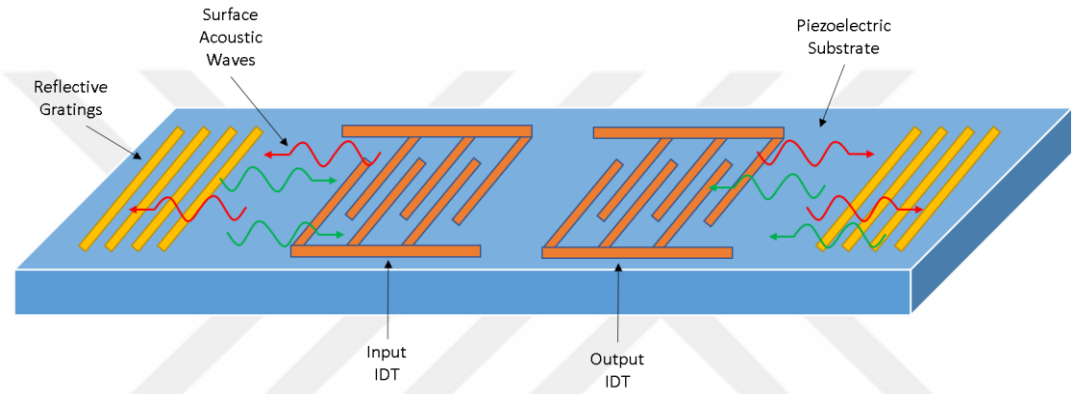

Figure 2.8. Two-port SAW resonator structure.

2.5.4 Delay Line

In terms of number of components, the delay line SAW configuration can be considered as one of the simplest configurations as it only has one IDT and reflective gratings on top of a piezoelectric substrate. A schematic of delay line structure of SAW device is depicted in figure 2.10. In this configuration a single IDT is used as input and also as output. This type of device generates the waves using the IDT. These waves are then reflected back to IDT by the reflective gratings that are found in the path of waves. The IDT then converts those waves to electrical signals. This type of configuration allows the receiver to calculate the time delay in between the waves which is directly related to the positions of reflective gratings on the device. This information can be utilized to identify the specific device in radio frequency identification (RFID) systems and also in sensor-based applications [116].

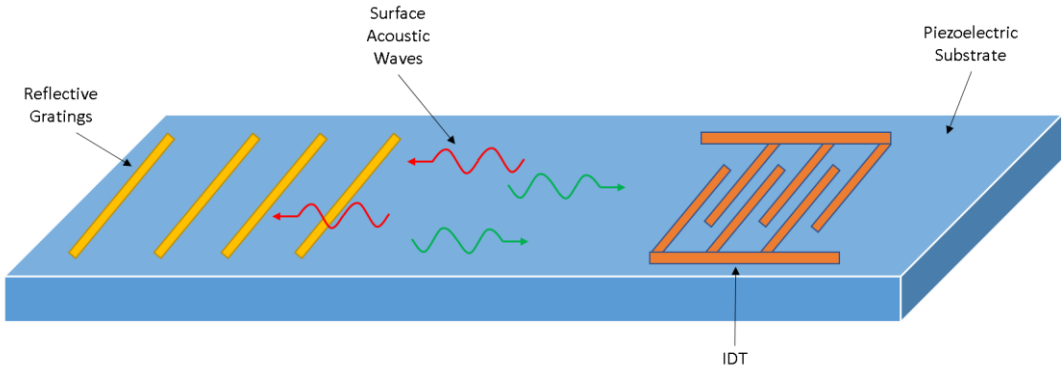

Figure 2.9. SAW device as a reflective delay line configuration.

Several other configurations of delay line-based SAW device exist [117]. Another form of delay line-based SAW device is presented in figure 2.11. This configuration employs two IDTs, one as an input and the other as an output IDT. The waves, after conversion from electrical to mechanical signals, travel from input to output IDT where they are converted back to electrical signals. The time taken by the waves to travel between IDTs is called delay time (τ) and can be calculated as:

$$\tau = \frac{x}{v_s}$$

Where,

x = Distance between input and output IDTs

v_s= Velocity of SAW

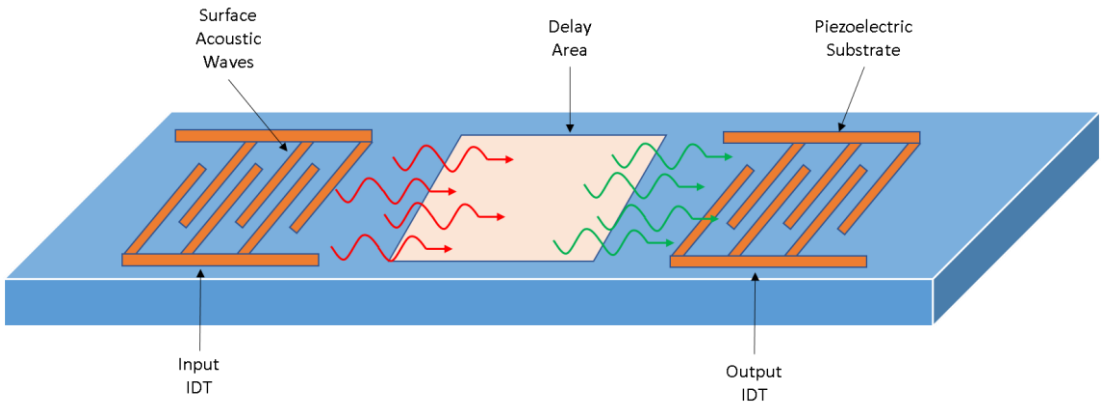

Figure 2.10. SAW as a delay line configuration.

2.6 Performance Evaluation Parameters for SAW Device

Any SAW device's performance can be evaluated using the following parameters:

- Insertion Loss
- Scattering
- Admittance
- Quality factor

Designing of a SAW device requires knowledge of those aforementioned parameters as they are directly related to the performance of the developed device. In the light of those parameters, the device design can be modified to achieve the desired performance.

2.6.1 Insertion Loss (IL)

Insertion loss, measured usually in dB, represents the power loss occurred during the signal transmission [118]. This type of loss happens due to the loss in reflection, dielectric and transmission medium. It is typically used to plot the frequency response of the device. It can be mathematically represented as:

$$IL = -20log_{10}|S_{21}|\ dB \tag{2.11}$$

OR

$$IL = -10log_{10}\frac{P_{out}}{P_{in}} \tag{2.12}$$

Where,

S_{21} = Transmitting parameter in dB

P_{out}= Output power in dB

P_{in}= Input power in dB

2.6.2 Scattering

Scattering parameters of S-parameters of a transmission system define its transmission and reflection characteristics in a frequency dependent matrix form [119]. The dimension of this matrix is directly equal to the number of ports of the transmission network.

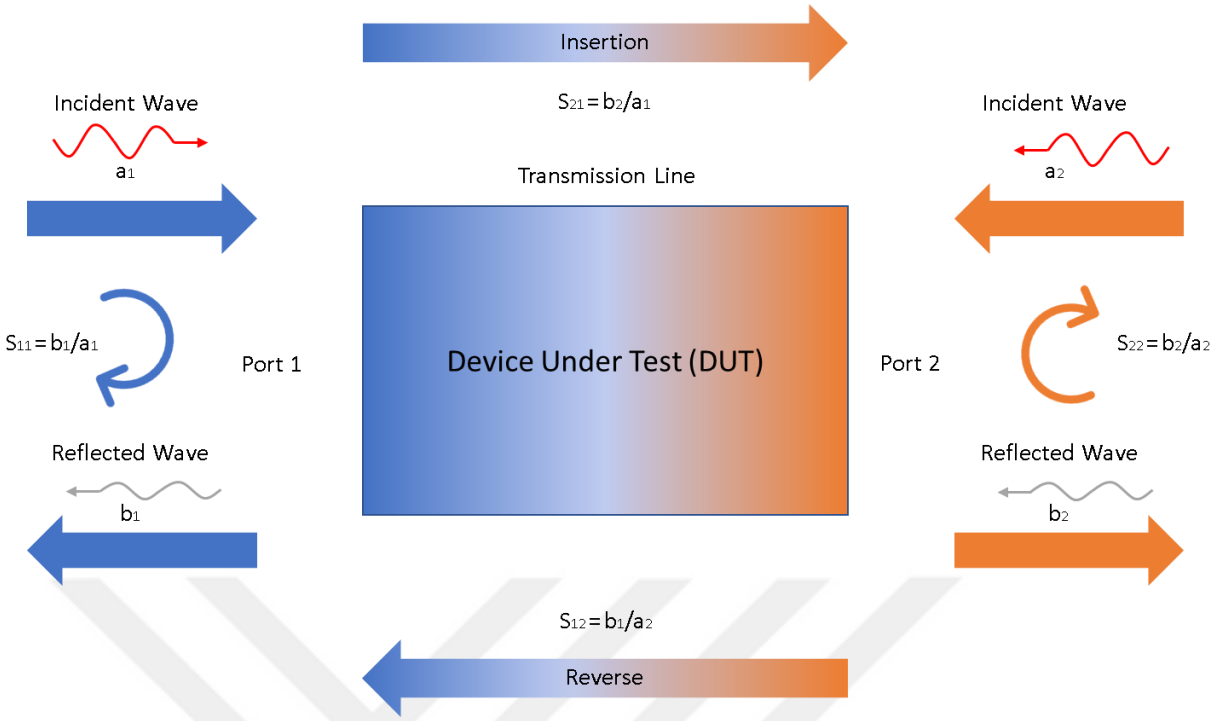

Figure 2.11. S-parameters for a two-port transmission system along with insertion and reverse parameters.

A two-port measurement of the signal flow is presented in figure 2.12. For a two-port transmission system, there are 4 S-parameters, S_{11}, S_{12}, S_{22} and S_{21}. The first number in the subscripts of S-parameter represents the output port of the signal while the second subscript shows the input port. S_{11} and S_{22} represent the input and output reflection of the signal while S_{21} and S_{12} show insertion and reverse transmission. Transmission equation in the form of a matrix can written as:

$$\begin{bmatrix} a_1 \\ b_1 \end{bmatrix} = \begin{bmatrix} S_{11} & S_{12} \\ S_{21} & S_{22} \end{bmatrix} \begin{bmatrix} a_2 \\ b_2 \end{bmatrix} \tag{2.13}$$

Where,

a_n = Incident wave

b_n = Reflected wave

2.6.3 Quality Factor (Q)

It is a dimensionless parameter that determines the level of damping for a resonator and can be defined as [114]:

$$Q = \frac{f_0}{\Delta f} \tag{2.14}$$

Where,

f_0 = Center frequency of the resonator

Δf = Bandwidth of the resonator

The higher the quality factor the narrower the bandwidth of the device thus producing an acute output in the region of center frequency hence increasing the sensitivity of the device. The quality factor and bandwidth of a SAW device are related to the number of electrode pairs of the input IDT for a specific center frequency [114].

$$\Delta f = \frac{2f_0}{N_p} \tag{2.15}$$

Where,

N_p = Number of input IDT electrode pairs

2.7 Sensing Physical Quantities using SAW

SAW-based sensing is basically realized by the changes in the characteristics of SAW propagation in relation to the quantity to be measured. This change can be observed as a fluctuation in IL or as shifting of centre frequency of the SAW based device. There are several factors which can cause the occurrence of one or both of those changes. These factors can be represented in the form of equation as follows [120]:

$$\Delta v_R = \frac{\partial v}{\partial m}\Delta m + \frac{\partial v}{\partial c}\Delta c + \frac{\partial v}{\partial \sigma}\Delta \sigma + \frac{\partial v}{\partial \varepsilon}\Delta \varepsilon + \frac{\partial v}{\partial T}\Delta T + \frac{\partial v}{\partial p}\Delta p + \cdots \tag{2.16}$$

Where,

Δv_R = Change in the velocity of Rayleigh waves

m = Mass

c = Stiffness

σ = Conductivity

ε = Dielectric Coefficient

T = Temperature

p = Pressure

Any of those aforementioned factors can result in the change of velocity of Rayleigh waves and hence using this principle a sensor can be developed. It is also possible to detect changes in more than one quantity by using an array of sensors [121–123]. Researchers have also showed that the use of array of sensors have a direct impact on increasing the sensitivity, accuracy, and selectivity of the sensing system [121, 124, 125]. Insights regarding the detection of aforementioned quantities are derived using the signature recognition techniques. Sensor arrays are also utilized for such purposes [121, 126–130]. Extended explanation regarding the measurement of some of those aforementioned quantities can be found in literature [131] while a brief introduction is provided below.

2.7.1 SAW based Temperature Sensing

Changes in temperature can affect the mechanical properties of the substrate. Since the velocity of SAW is directly affected by the changes in mechanical properties of the substrate hence those changes can be derived to reflect the temperature measurements [132–134]. The selection of substrate material depends upon the physical environment where the sensor will be deployed. In general, a substrate with a temperature coefficient of zero is preferred still different materials are also used [135].

2.7.2 SAW based Pressure Sensing

Pressure sensing using SAW-based device relies on the induction of strain over the substrate [136–138]. This type of sensing is generally susceptible to environment parameters which can affect the accuracy of measurement. In order to overcome this problem a reference sensor is deployed in a differential setting [139]. That sensor can act as a reference to increase the accuracy of the system.

2.7.3 SAW based Conductivity Sensing

Conductivity measurement using SAW-based sensor is a popular technique for the detection of gas and chemical compounds [140, 141]. Conductivity measurement using SAW is performed by depositing a thin layer of conductive film over piezoelectric substrate. This conductive film is active towards the target compound or gas. Following mathematical equations describes the effect of conductivity on SAW velocity [120]:

$$\frac{\Delta f}{f_0} = \frac{\Delta v}{v_R} \cong \frac{-K^2}{2} \frac{\sigma_S^2}{\sigma_S^2 + v_0 C_S^2} \tag{2.17}$$

Where,

Δf = Shift in frequency

f_0 = Center frequency of SAW device

v_R = SAW velocity at normal condition

K^2 = Electromechanical coupling coefficient of substrate

σ_S^2 = Surface conductivity of the deposited sensing film

C_S = Capacitance per unit length of the surface

The effect of electro-acoustic attenuation can be described by the following equation [120]:

$$\frac{\alpha}{k} \cong \frac{K^2}{2} \frac{v_R\, C_S\, \sigma_S^2}{\sigma_S^2 + v_R^2 C_S^2} \tag{2.18}$$

Where,

α = Electro-acoustic attenuation

k = Wave number

2.7.4 SAW based Mass Load Sensing

SAW-based sensors are implemented as biosensors and chemical sensors as they are sensitive to the accumulated mass on their surface. SAW devices for mass load detection

is based on the detection of changes in the center frequency of the device [142–144]. The following equation is used to define mass sensitivity [145]:

$$S_m = \lim_{\Delta m \to 0} \frac{(\Delta v / v_R)}{\Delta m} = \lim_{\Delta m \to 0} \frac{(\Delta f / f_0)}{\Delta m} \tag{2.19}$$

Where,

S_m = Mass sensitivity factor

Δm = Mass per unit area

3 DESIGN AND FABRICATION METHODOLOGY

3.1 Sensor Design

The design of the proposed single port IDT structure along with its parameters is presented in figure 3.1. The aperture of the proposed device is represented as A and the distance between the two IDTs, i.e. wavelength, is depicted by λ_0. The details of all the parameters are defined in table 3.1.

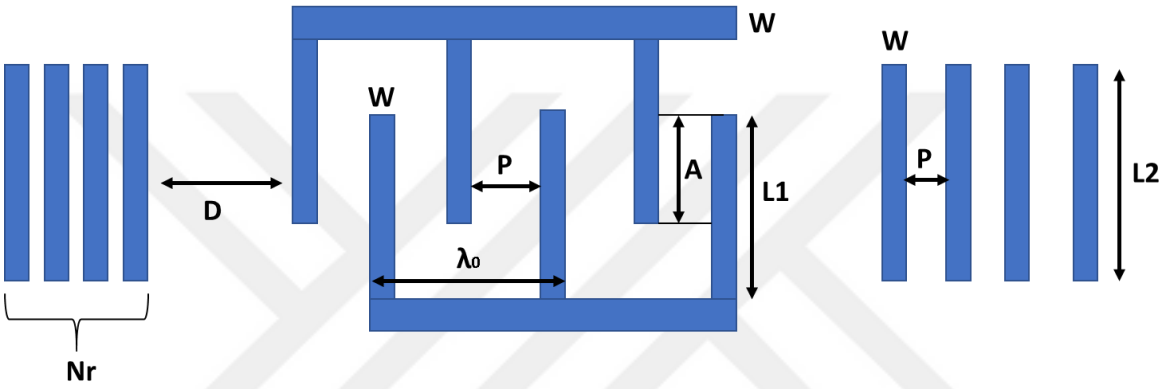

Figure 3.1. Design and design parameters of the proposed IDT sensing structure.

Table 3.1. Summary of geometric parameters for the proposed IDT structures

Measurement Name	mm	µm
Thickness of the whole design	0.002	2
Electrode finger width (W)	0.003	3
Distance between electrodes (P)	0.003	6
IDT length (reflectors) (L2)	0.08	80
IDT length (L1)	0.1	100
Distance between IDT and Reflectors	0.003	3
Distance between two IDTs (λ0)	0.015	21
Aperture (A)	0.092549	92.549
Number of Reflectors (Nr)	15	
Number of IDT Pairs (Ni)	30	

Figure 3.1 describes the structural design parameters for the proposed SAW resonator-based temperature sensor. As depicted in figure 3.1, the IDT structure is designed with a certain pitch among them and the resulting surface acoustic wave is well-founded when the pitch of the IDT fingers and the wavelength of the surface wave are equal to each other. Equation 3.1 is employed to determine the resonant frequency (f), which is a function used for measuring temperature, of the proposed structure and its relation to the propagation velocity (v_R) of the resulting surface wave.

$$f = \frac{v_R}{\lambda_0} \tag{3.1}$$

Where,

λ_0 = Wavelength of the SAW

The IDT structure needs to be quantified in order to develop its model. Figure 3.1 and table 3.1 show the labelled IDT structure and its explanation respectively. In order to achieve the strongest IDT activation and phase superposition of SAW, the IDT pitch, which is $W + P$, should be equal to half of the SAW wavelength, as described by the wave interference principle. Therefore,

$$W + P = N\frac{\lambda_0}{2} \tag{3.2}$$

The distance between the IDT and the adjacent reflectors should also satisfy equation 3.3 to make sure that IDT receives the standing wave on its peak.

$$D = \left(N - \frac{1}{2}\right)\frac{\lambda_0}{2} \tag{3.3}$$

Aperture width of the IDT fingers also plays an important role in the performance of the SAW resonator. Normally, it is between 50 and 100 times the SAW wavelength [146].

3.2 Fabrication

The advancements in the field of 3D printing techniques started to pick up pace in 1980s in order to make the fabrication of customized complex structure easier and less time consuming [147, 148]. Since its introduction, it has gained popularity and applications in

many fields such as construction [149], medical industry [150], and even food preparation [151]. There are many different types of 3D techniques being utilized throughout the world for many applications and among them is Two-Photon Polymerization (2PP). 2PP allows increase in spatial resolution because of the photochemical reaction in photoresist caused by the laser light [152, 153]. 2PP is based on photon excitation phenomenon [154] which was experimentally proved after the development of pulsed lasers in 1961 [155]. Fabrication using 2PP [156, 157] was evolved in 90s [158] and has found its application in many different fields including but not limited to biosensing [159, 160], optics [161–163], robotics [164–166], and biomedical [167–169]. Direct Laser Write (DLW) based 2PP printing technique [170] was utilized for this study.

Nanoscribe GmbH's Photonic Professional GT photopolymerization based setup was utilized for the fabrication of the sensing structure. The fabrication setup is based on a DLW system using 2PP. This system implements a femtosecond fibre laser source which is operating at 780 nm wavelength. The power of the deployed laser source was between 50 – 150 mW with 80 MHz of repetition rate. The laser source uses a pulse length of 100 – 200 femtoseconds. A general representation of the setup is shown in figure 3.2.

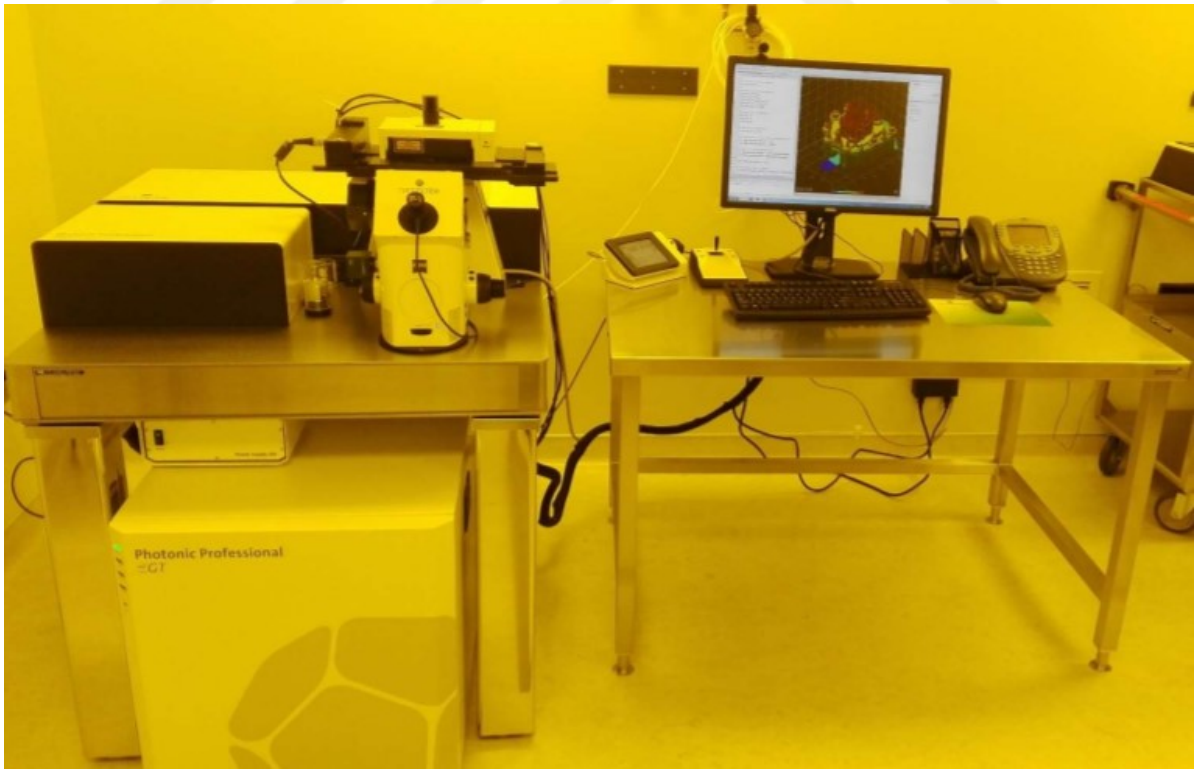

Figure 3.2. Nano 3D printer - Nanoscribe Photonic Professional GT

The 3D printer shown in figure 3.2 has the ability to fabricate both 2D and 3D structures from nano to micron scale. The printer can be operated using Dip-in Liquid Lithography (DiLL) or Direct Laser Write (DLW) modes. For this study, DLW mode was utilized using 63x objective for high-resolution fabrication.

DLW mode allows the printing of nanostructures up to 100 nm feature size. DLW uses a Near-Infrared (NIR) laser on a photoresist, which is UV sensitive, thus causing a very specific photochemical reaction. Using this technique with 2PP, objects with resolution less than 100 nm can be fabricated [153, 171, 172]. The fabrication of the sensing structures was realized using the Nanoscribe's Photonic Professional GT printer which is available commercially and allows the 3D fabrication using DLW 2PP system. The overview of the setup is provided in figure 3.3.

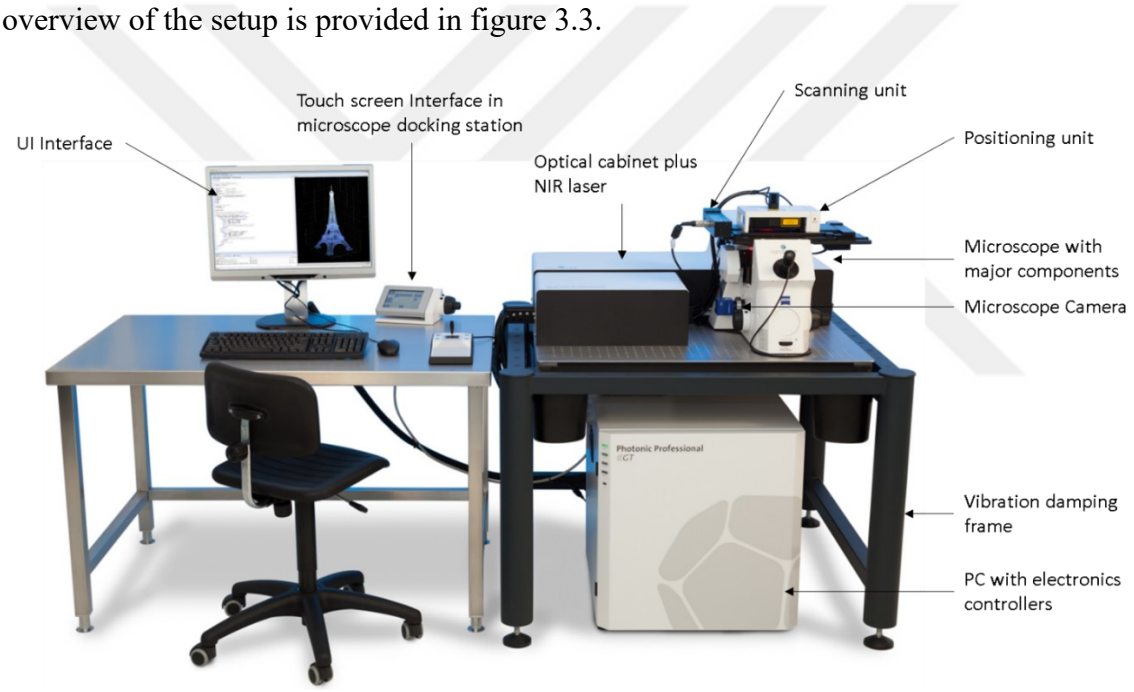

Figure 3.3. System setup overview of the Nanoscribe's Photonic Professional GT.

As shown in figure 3.3, one of the main components of the systems is the inverted microscope which has a piezoelectric self-balancing stage on top of it. The laser source is located just beside the optical cabinet and consists of an erbium-doped fiber laser. The wavelength of the laser is 780 nm and it can produce pulse with a pulse length between 100 to 200 femtoseconds with 80 MHz repetition rate. The power of the deployed laser can be between 50 to 150mW. The intensity of the laser can be adjusted using an acousto-optic modulator and by precisely focusing the beam towards the UV-curable photoresist with the help of an objective lens. The system can be configured to operate in either DiLL

or DLW modes. For this study, the system was operated in DLW mode and scanning was done using galvo scan mode to speed up the fabrication process. Power intensity of the laser, deployed objective along with the scan speed are all the factors that determines the occurrence polymerization during a 2PP process. The working principle of the system is illustrated in figure 3.4 [173] below:

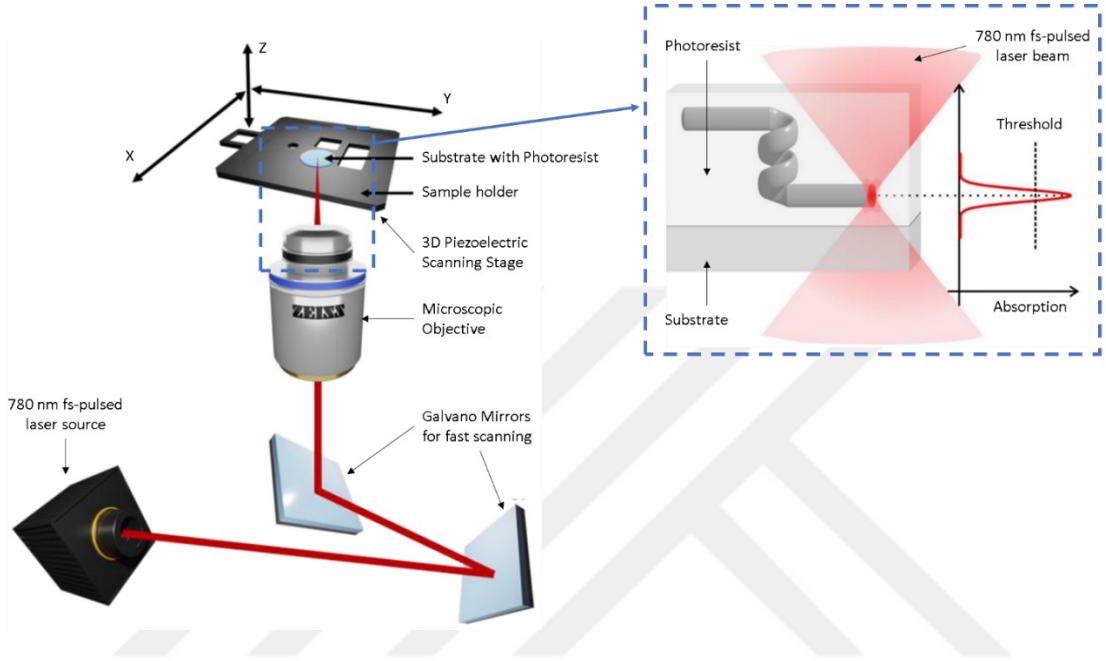

Figure 3.4. Working principle schematic of 2PP based DLW printing method.

The workflow for printing a part using Photonic Professional GT printer is shown in figure 3.5. The whole process can be divided into 3 main parts that is, Preparation, Production and Post-Processing. Details of the process are presented below:

1. First of all, the design to be printed is prepared using a CAD design software. For this study Siemen's NX was utilized.
2. The design is then converted to .stl file format.
3. The converted .stl file is uploaded to Describe software which is used for converting .stl file to .gwl file. The design is now reading to be shifted to production phase of the workflow.
4. Next, the parameters for the printing are configured. Type of objective utilized, scaling, and orientation are some of the parameters that can be selected here. For this study, 63x/1.4, a microscope objective from Carl Ziess, an oil immersion objective was used. Two of the most important parameters that define the power of the laser source and its movement are laser power and scan speed.

5. Finally, the desired structure is sent for printing.

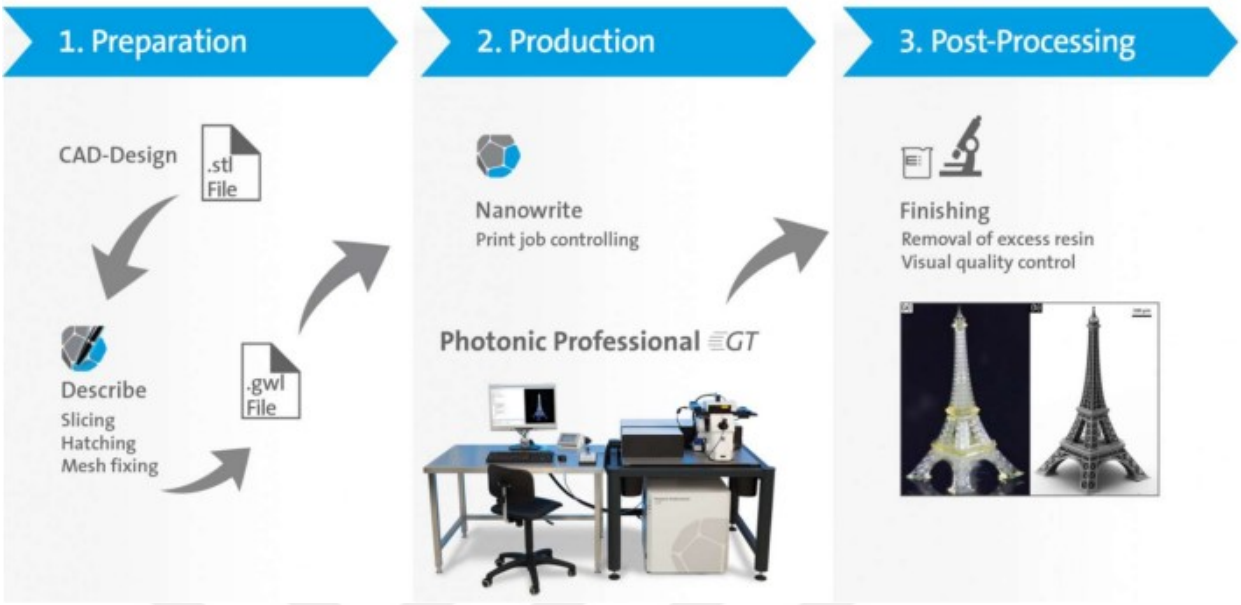

Figure 3.5. Fabrication workflow for Photonic Professional GT.

Figure 3.6 illustrates the 3D printing for using DLW or oil immersion-based fabrication. In this configuration, the resin is deposited on the glass substrate. For printing using 63x/1.4 microscope objective, a drop of immersion oil with matching refractive index to that of the substrate is applied on the objective. Therefore, a laser beam from femtosecond pulsed laser is directed into the photoresist through the focusing objective. The desired structure is printed additively from the substrate level and its maximum height is 190 µm for 63x/1.4 microscope objective.

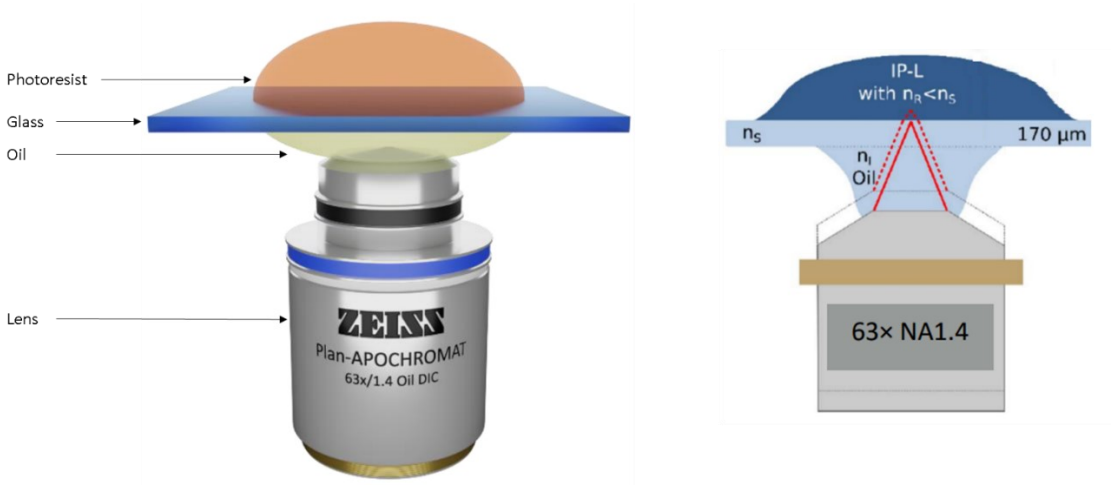

Figure 3.6. Schematics of DLW based 3D printing setup.

3.3 Model Development:

The CAD of the proposed IDT structures were prepared using Siemens' NX and klayout editor programs. The output of the models developed using those two programs are shown in figures 3.7 and 3.8.

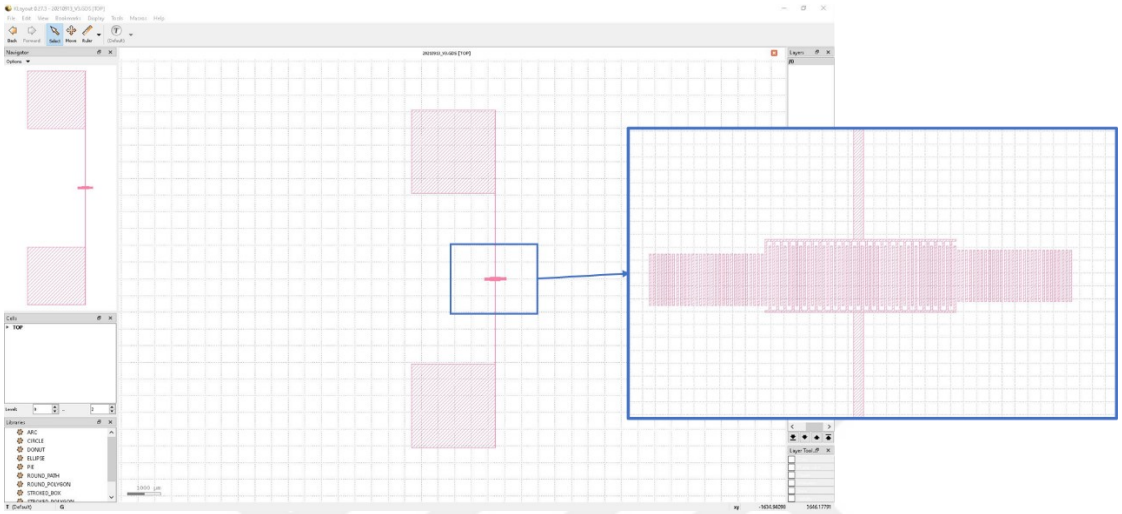

Figure 3.7. Developed model of the IDT structures using klayout editor.

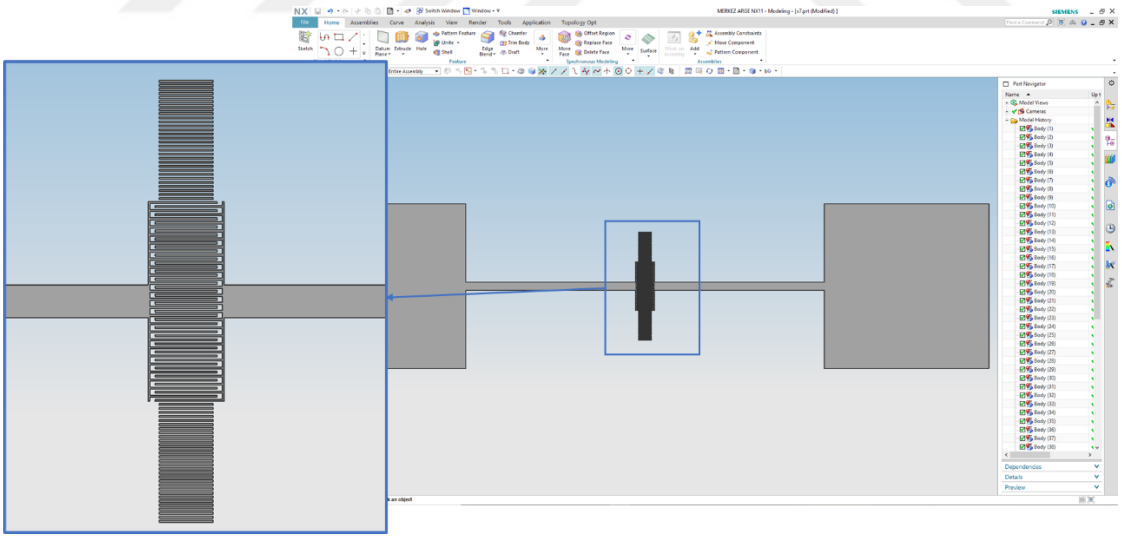

Figure 3.8. Developed model of the IDT structures using Siemens NX.

4 RESULT AND DISCUSSION

4.1 Fabrication Process

The fabrication process is based on the workflow described in figure 3.5. First of all, a CAD software, Siemens NX, was used to create the desired structure. The designed structure was then saved as .stl file and imported to Describe software where it was converted to .gwl format. Printing parameters were defined and finally the printing was performed. The image of system is shown in figure 4.1.

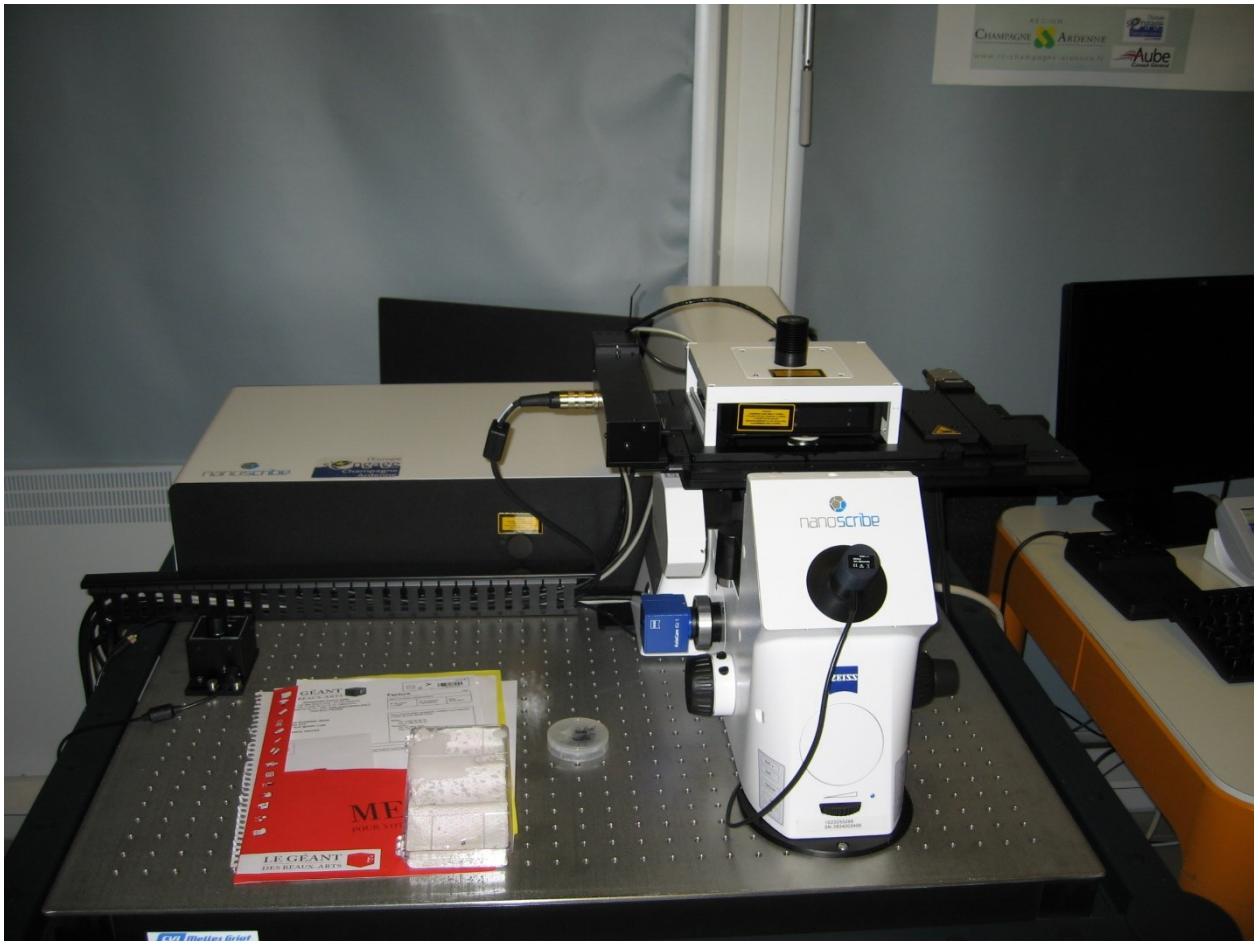

Figure 4.1. Image showing the utilized Nanoscrbie 3D printing system.

In order to focus the laser light on to the sample Plan-APOCHROMAT 63x/1.4, a microscope objective from Carl Ziess, an oil immersion objective was used. The magnification and the numerical aperture of the objective was 63x and 1.4 respectively.

Figure 4.2. Microscope oil immersion objective from Carl Ziess.

The dimension of the glass substrate used for this fabrication process was size 22 mm x 22 mm with a thickness of 170 µm. The substrate was cleaned before the realization of the printing process. The cleaning process involved ultrasonic cleaning using acetone and isopropanol. The substrate was then blow-dried using air in order to make it ready for the printing.

Later on, 60% v/v of MICROPOSIT S1813 EC solvent 11 positive photoresist was deployed on the surface of the substrate. The sample was then spin coated on to the substrate at 4000 RPM for 30 seconds using Karl Suss CT62 spin coating machine. After the completion of the spin coating process, a layer of approximately 500 nm in thickness was achieved. While exercising precautions, the sample was developed using MF-319 developer solution for about 30 seconds at room temperature. Finally, the sample is then cleaned by soaking in de-ionized water. Conductive IDT structures were generated by Plassys MEB400 machine depositing 5 nm thick chromium and then 30 nm thick gold at ±15° angles with respect to substrate. In order to remove the remaining photoresist from the sample a lift-off process was employed by immersing the prepared sample into acetone and keeping it there for 10 hours. Finally, the sample is then rinsed using de-ionized water and blow-dried using air.

The workflow described above and followed during the fabrication process proved successful and several temperature sensing structures were generated using 2PP DLW micro fabrication technique. The IDT structures were fabricated out of Gold and the

printing was performed using Nanoscribe's Photonic Professional GT system. The results of the printing are shown in figure 4.3.

Figure 4.3. Picture of the fabricated IDT structures.

Zeiss's Smartzoom 5 was utilized to inspect the fabricated IDT structures. A picture of the setup is shown in figure 4.4.

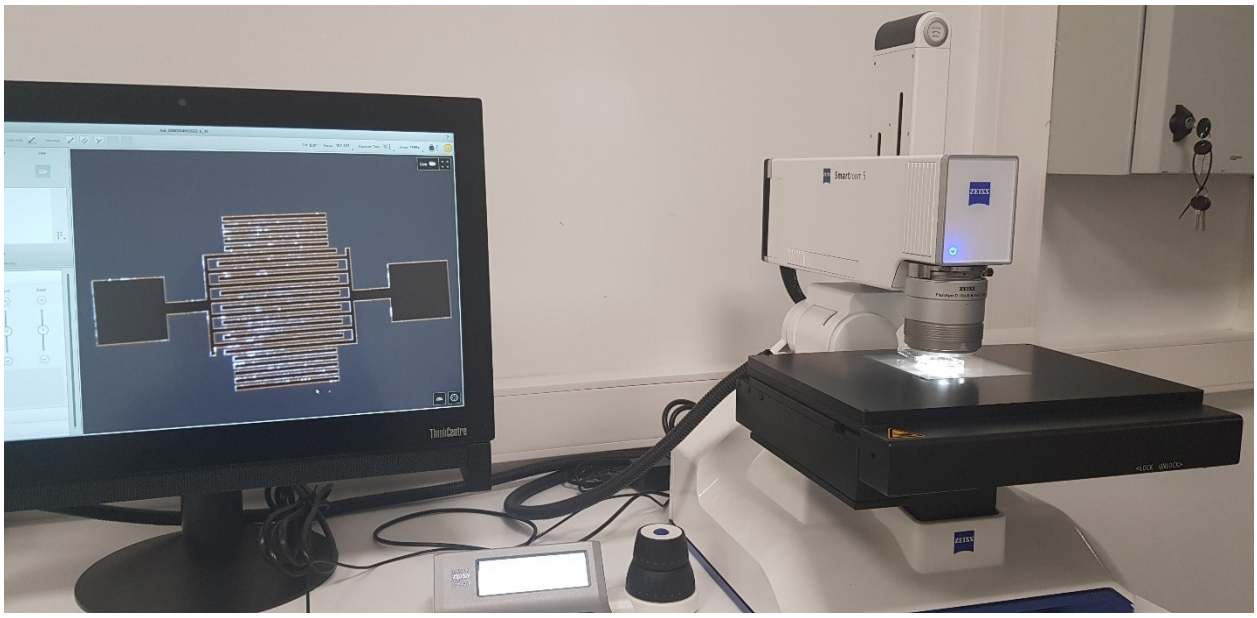

Figure 4.4. Inspection of the fabricated IDTs using Zeiss's Smartzoom 5 digital electron microscope system.

The fabricated IDT structures can be seen under the electron microscope in figure 4.5.

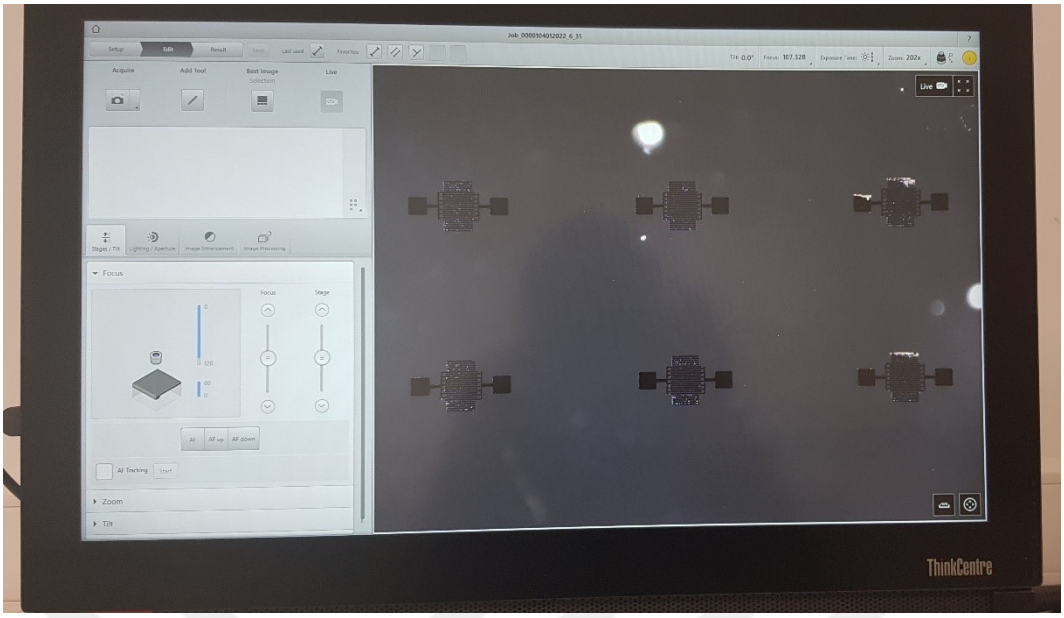

Figure 4.5. Fabricated IDT structures during the examination under the electron microscope system.

Zoomed in images of the fabricated IDT structures can be seen from figure 4.6 to figure 4.11.

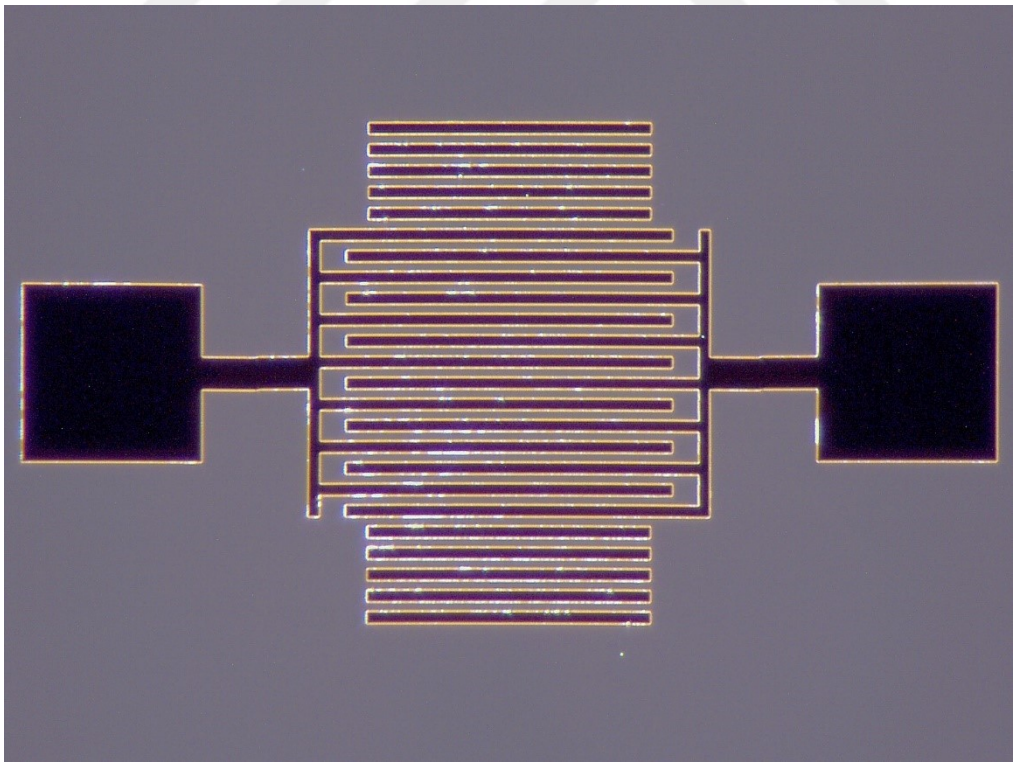

Figure 4.6. Electron microscope image of the fabricated IDT No. 1.

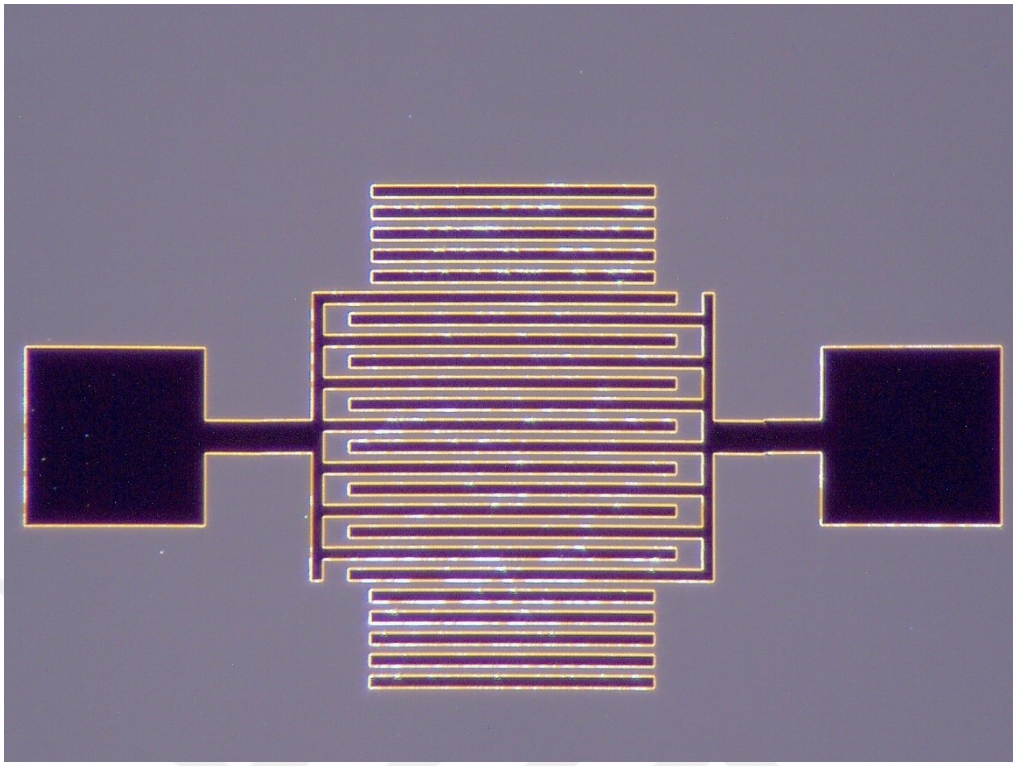

Figure 4.7. Electron microscope image of the fabricated IDT No. 2.

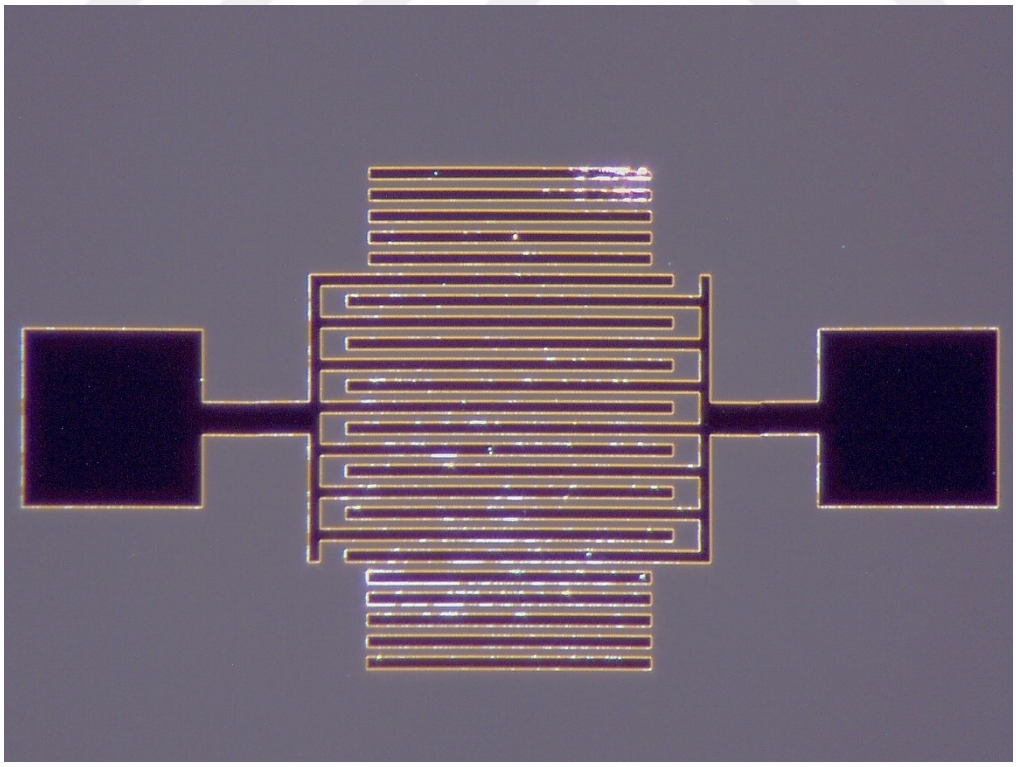

Figure 4.8. Electron microscope image of the fabricated IDT No. 3.

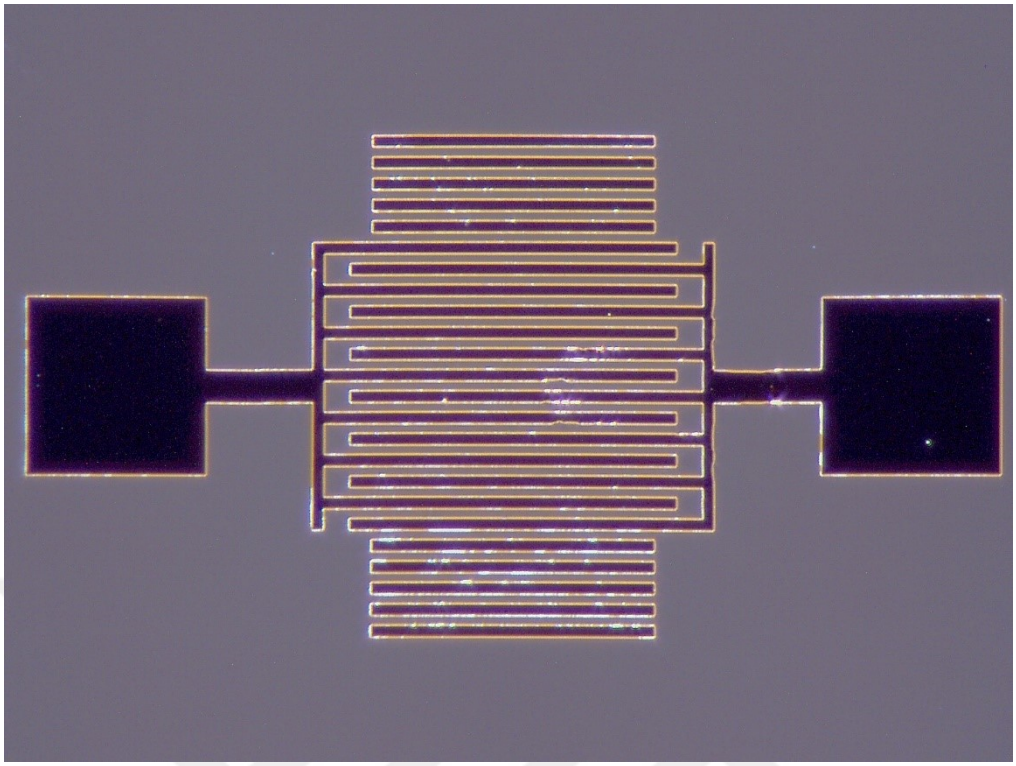

Figure 4.9. Electron microscope image of the fabricated IDT No. 4.

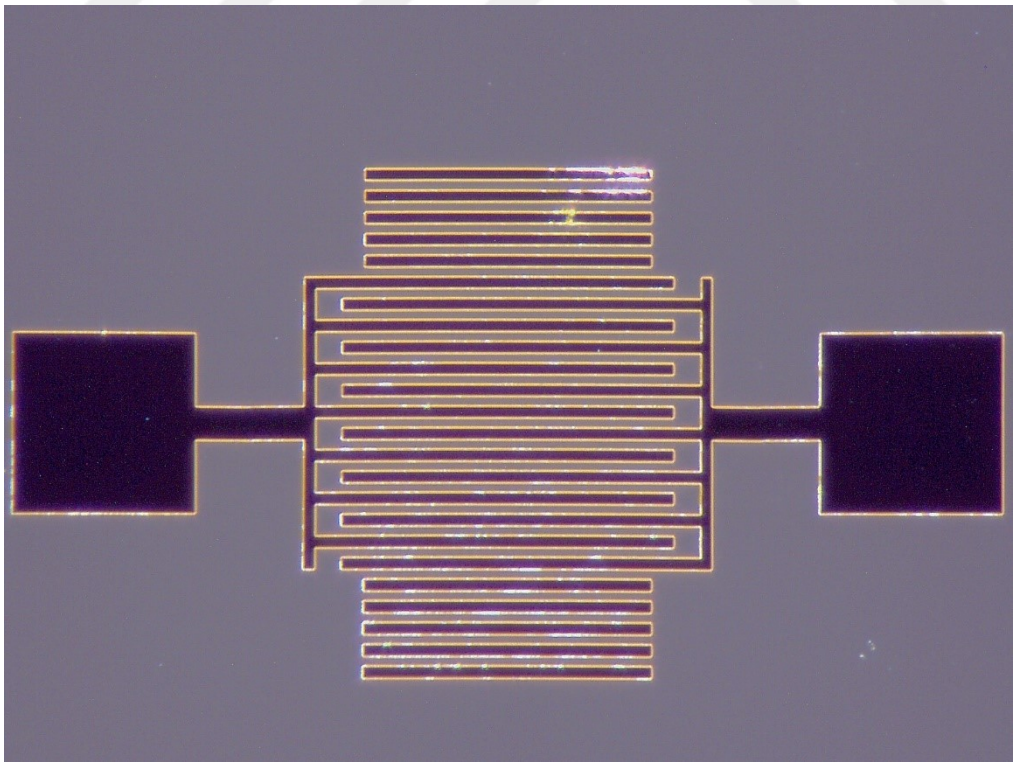

Figure 4.10. Electron microscope image of the fabricated IDT No. 5.

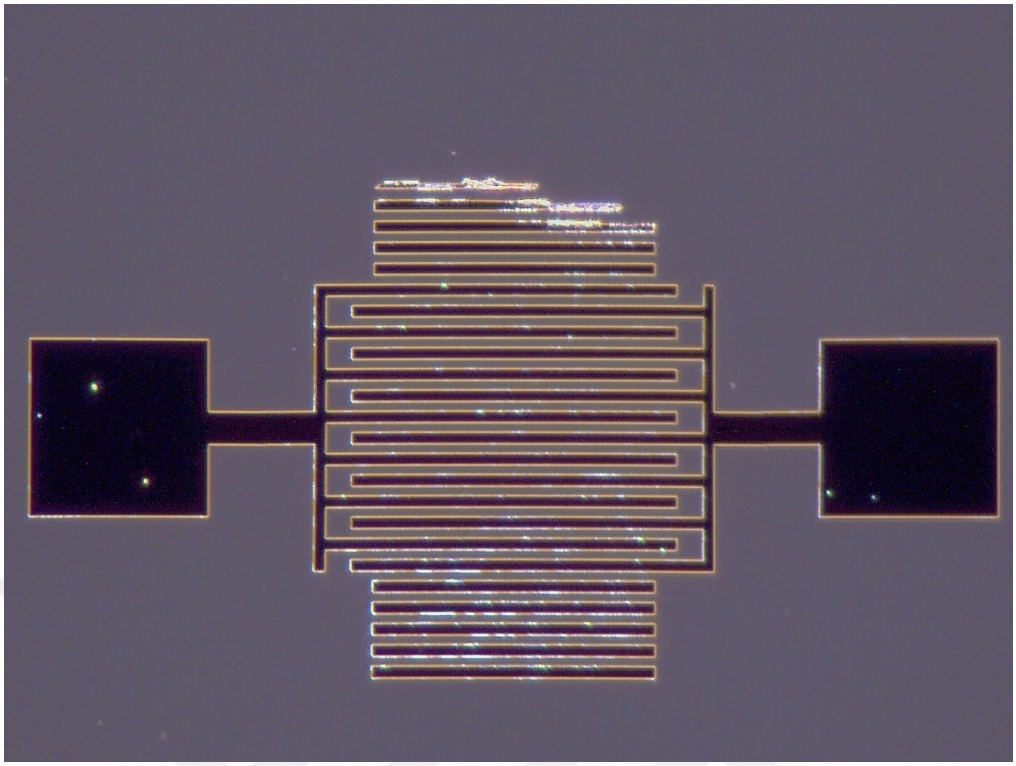

Figure 4.11. Electron microscope image of the fabricated IDT No. 6.

In addition to the inspection of the fabricated IDT structures using electron microscope, inspection using Scanning Electron Microscopy (SEM) was also performed. The results of this are presented in figure 4.11.

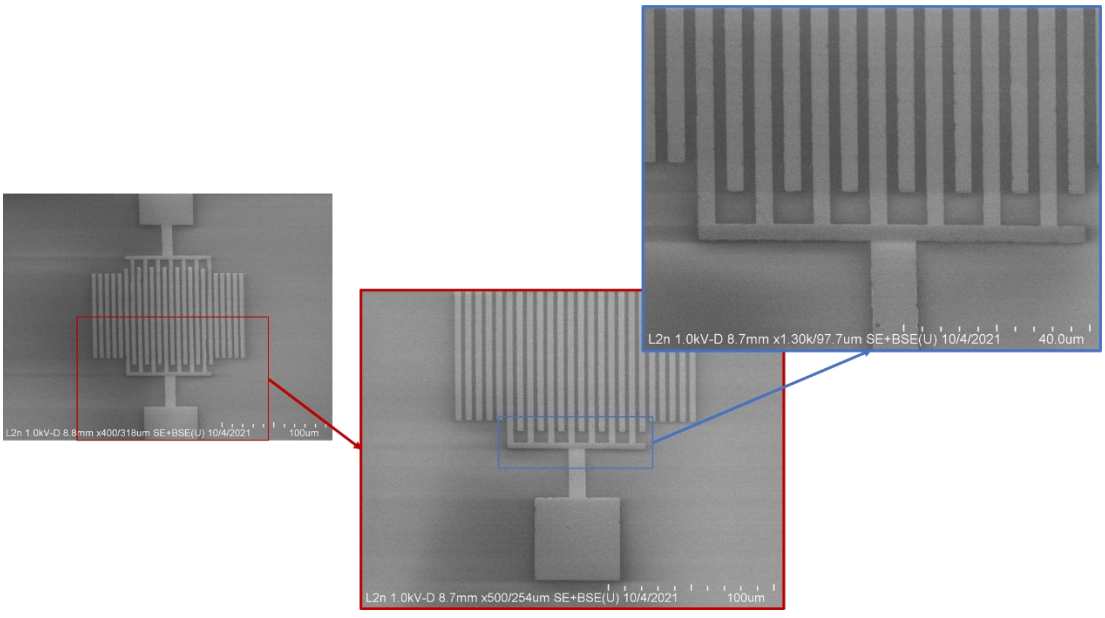

Figure 4.12. SEM image of the fabricated IDT structure.

4.2 FEA Analysis and Simulation:

The finite element analysis of the proposed SAW-based temperature sensing devices is performed using COMSOL Multiphysics. This software a versatile and efficient simulation conditions along with a user-friendly interface. Partial differential equations that forms the governing principle are applied for the simulation.

Analyzes were performed using the MEMS toolbox of the COMSOL program because of its exclusive piezoelectricity interface which makes it a perfect fit for the simulation of SAW. The MEMS toolbox of the software covers all the required tools that are necessary for the simulation.

The basic analysis steps related to this program are given in this section. The properties of material, i.e. elasticity matrix, coupling matrix, and relative permittivity, must be clearly defined for the analysis of any piezoelectric based device using COMSOL. The COMSOL Multiphysics Platform consists of the following steps for MEMS analysis:

- Initialization of the software
- Definition of the parameters
- Construction of geometrical structures
- Material definitions
- Mesh attribution
- Configuration the work

The results of those analyses are used to simulate and thus evaluate the performance of those devices. The configuration of the proposed devices is described in section 3. The analysis can be performed using a pair of electrode fingers, since IDTs are periodic, for displacement. Again, using the boundary conditions, the aperture of the device can be assumed infinite reducing it to a few of the wavelength.

4.3 Implementation of SAW using Gold Electrodes

The resonance frequency of the SAW-based resonator is calculated via piezoelectric material and eigenfrequency which in turn determines the velocity of the SAW in the designed structure. Quartz structure with the following constants [174–180] are used for this study. Equations 4.1 defines the elasticity matrix as E:

$$E = \begin{bmatrix} 8674 & 698 & 1191 & -1791 & 0 & 0 \\ 698 & 8674 & 1191 & 1791 & 0 & 0 \\ 1191 & 1191 & 10720 & 0 & 0 & 0 \\ -1791 & 1791 & 0 & 5794 & 0 & 0 \\ 0 & 0 & 0 & 0 & 5794 & -1791 \\ 0 & 0 & 0 & 0 & -1791 & 3988 \end{bmatrix} X\ 10^9\ GPa \qquad (4.1)$$

The coupling matrix is shown in equation 4.2 as C:

$$C = \begin{bmatrix} 17.1 & -17.1 & 0 & -4.06 & 0 & 0 \\ 0 & 0 & 0 & 0 & 4.06 & -17.1 \\ 0 & 0 & 0 & 0 & 0 & 0 \end{bmatrix} X\ 10^9\ C/m^2 \qquad (4.2)$$

The relative permittivity, ε, is described in equation 4.3 as:

$$\varepsilon = \begin{bmatrix} 392.1 & 0 & 0 \\ 0 & 392.1 & 0 \\ 0 & 0 & 410.3 \end{bmatrix} X\ 10^9\ F/m \qquad (4.3)$$

The density is 2.649 g/cm^3 while Poisson's ratio is 0.17 and Young's modulus is 76.5 GPa. The usage of the periodic boundary condition implies that the electrical potential and the displacement are identical along both the vertical sections of the model.

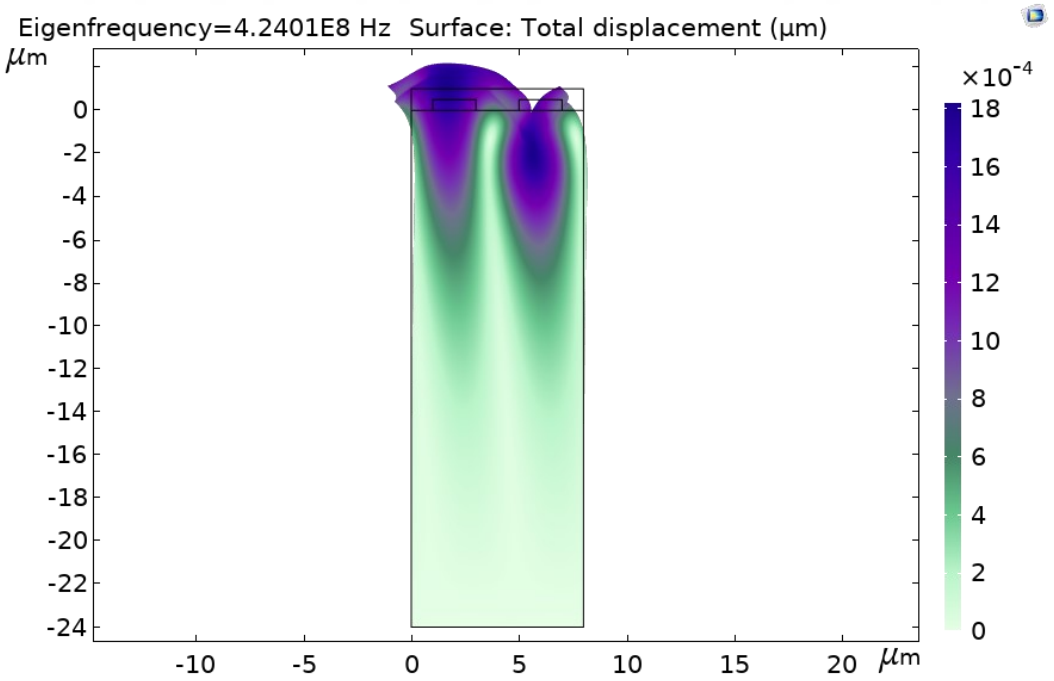

Figure 4.13. Resonant frequency mode plot of IDT structures with gold electrodes.

The results of the analysis show the resonant frequency, shown in figure 4.13, for the proposed IDT structure to be 424.01 MHz. The anti-resonant frequency, depicted in figure 7, is 426.69 MHz.

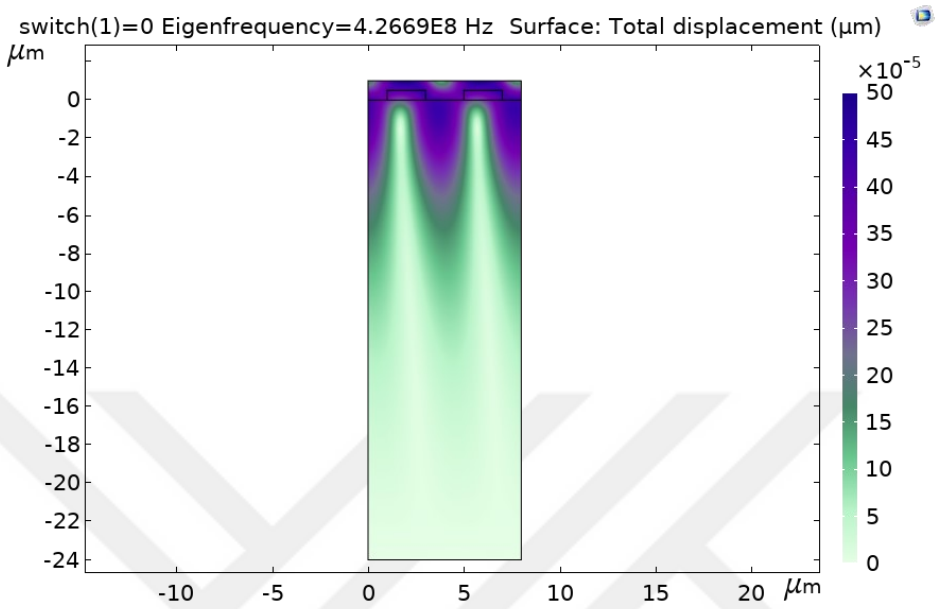

Figure 4.14. Anti-resonant frequency mode plot of IDT structures with gold electrodes.

Considering the first and second eigenfrequencies of the SAW modes, shown in figures 4.13 and 4.14, the electric potential distribution characteristics according to the illustrated solutions are shown in figure 4.15 below.

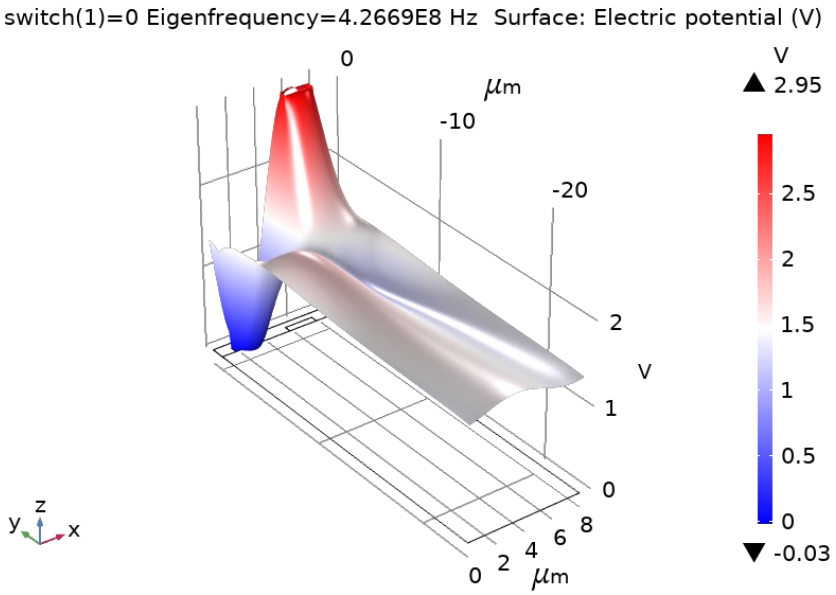

Figure 4.15. Electrical potential distributions at the 2nd eigenfrequencies

The electricals response of the proposed device is presented in figure 4.16. It can be seen from the graph that when an electrical potential is applied to the IDTs the device experience strain in its piezoelectric substrate and produce SAW that travels across the surface and thus causing deformation in the structure.

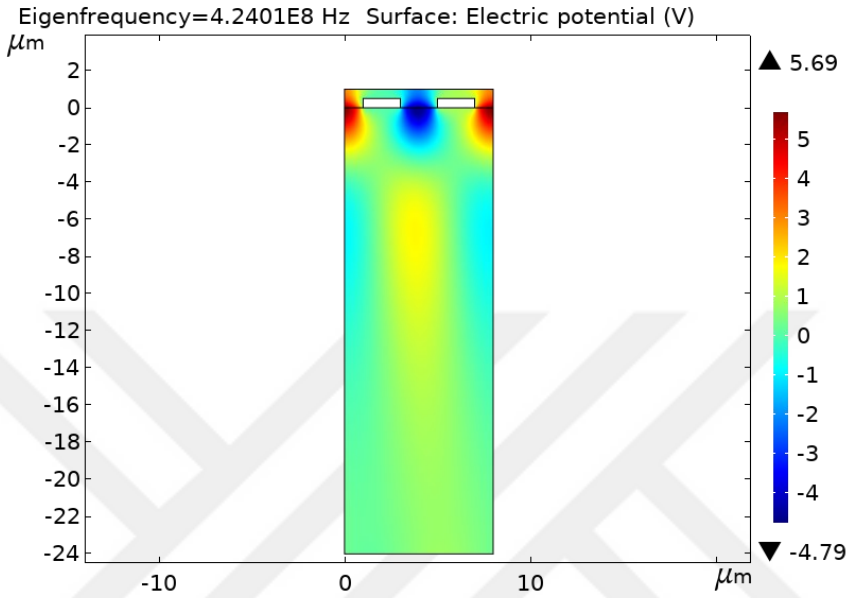

Figure 4.16. Surface electrical potential response of the IDT structure

Electric potential distribution and mechanical vibration mode at the resonance frequency can be obtained by utilizing the coupling between the electric and mechanical fields. The electrical potential at the resonance frequency is shown in figure 4.7. Similarly, the mechanical vibration characteristics using the simulation techniques are shown in figures 4.13, 4.14, and 4.15.

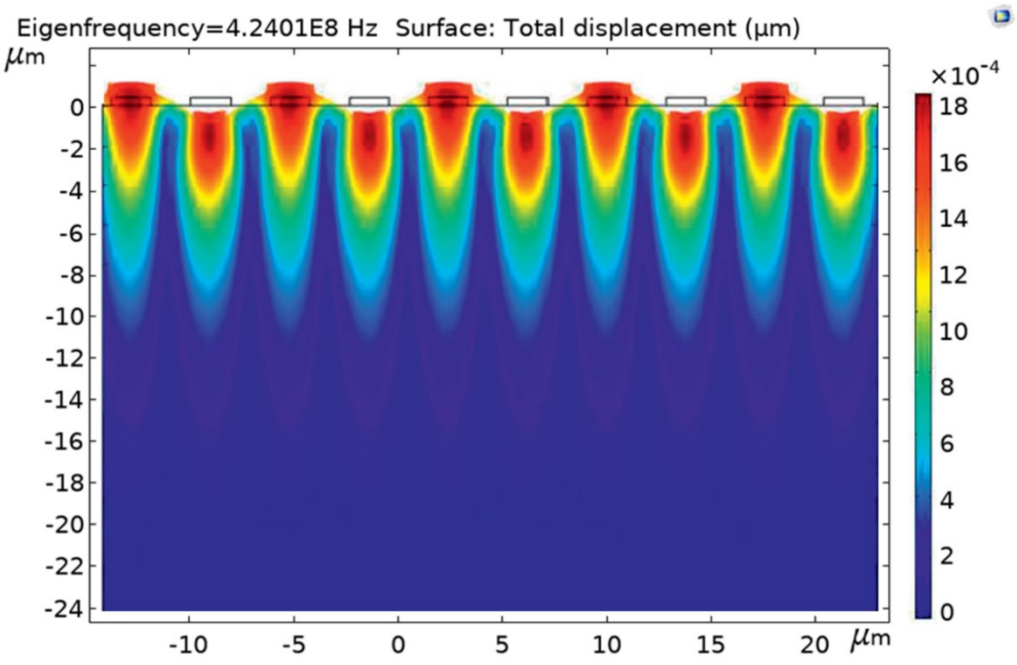

Figure 4.17. Surface displacement response of the IDT structures.

4.4 Resonance Frequency Measurements

The fabricated IDT structures, shown in section 4 with their design parameters described in section 3, were tested using network analyzer in order to measure their frequency response and to check their resonance frequency practically. The general representation of the setup in shown in figure 4.18.

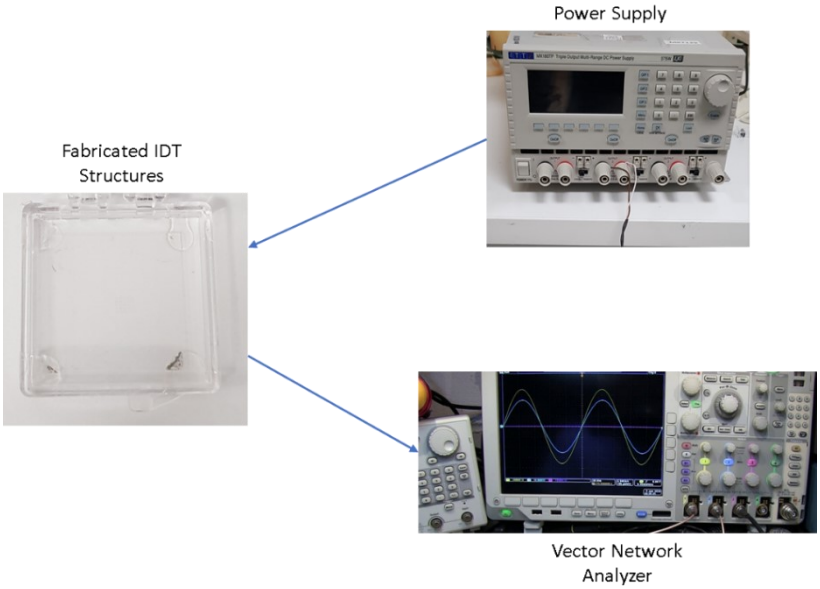

Figure 4.18. Setup for resonance frequency measurement.

The frequency response of the developed sensor is shown in figure 4.19. The resonance frequency of the designed structure was found to be 424.01 MHz according to the theoretical calculations and simulations, shown in figures 4.13, 4.14, 4.16 and 4.17. From the practical experiments, the value of resonance frequency is measured as 426.2 MHz, as illustrated in figure 4.19. Comparing these two results, the error is calculated to be 0.5% which is well within the acceptable range. The graph is figure 4.19 shows the consistency in theoretical design and the fabricated structures.

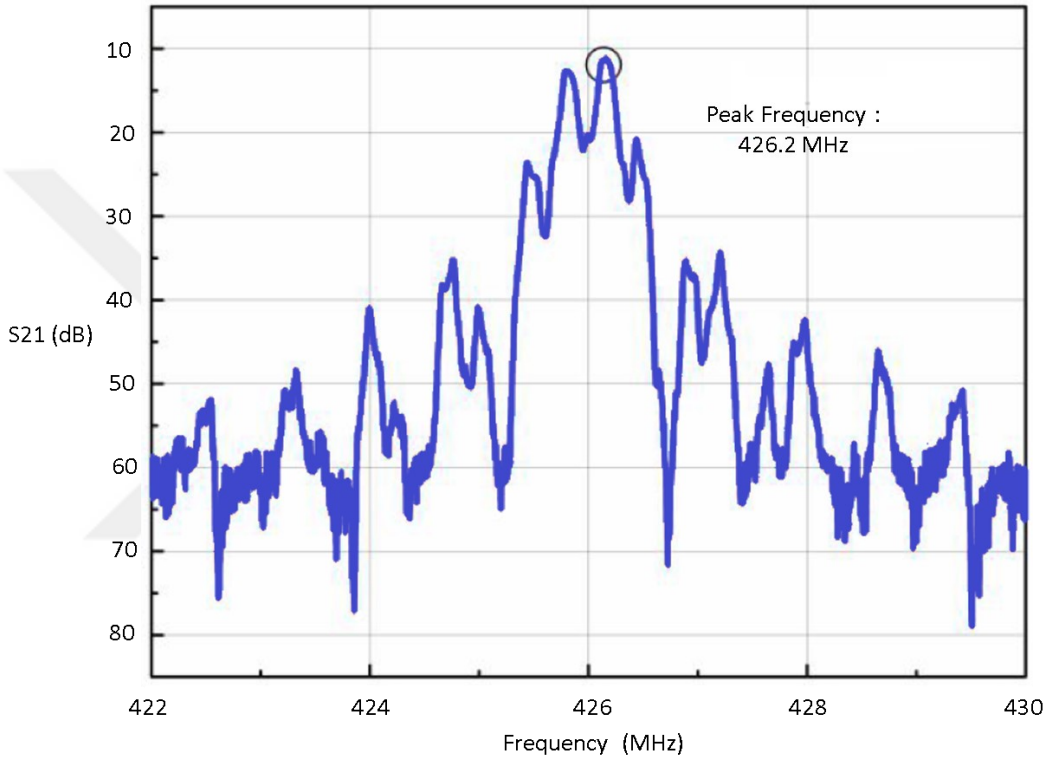

Figure 4.19. Frequency response of the fabricated IDT structures.

4.5 Temperature Response of IDTs:

The fabricated IDT structures are then tested for their application to measure temperature. The illustration of the test setup is shown in figure 4.20. The climatic test chamber allows an easier and precise control of the temperature.

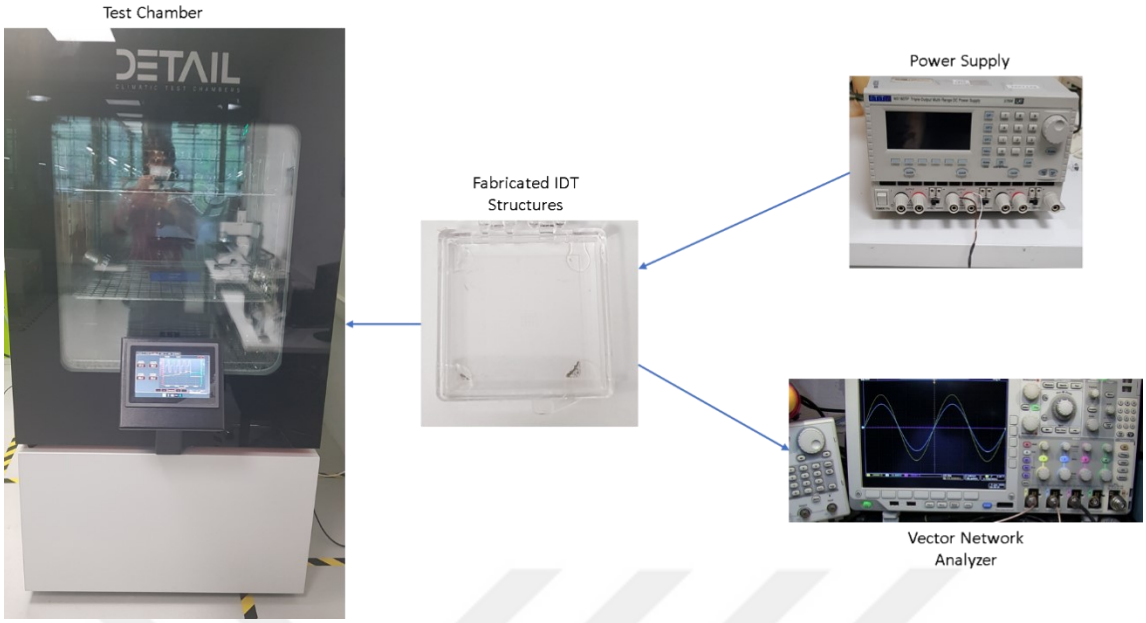

Figure 4.20. Setup for temperature response measurement of the fabricated IDT structures.

The frequency response of the fabricated IDTs, 6 in total, were scanned and noted. The results are presented in figures 4.21 to 4.27 below.

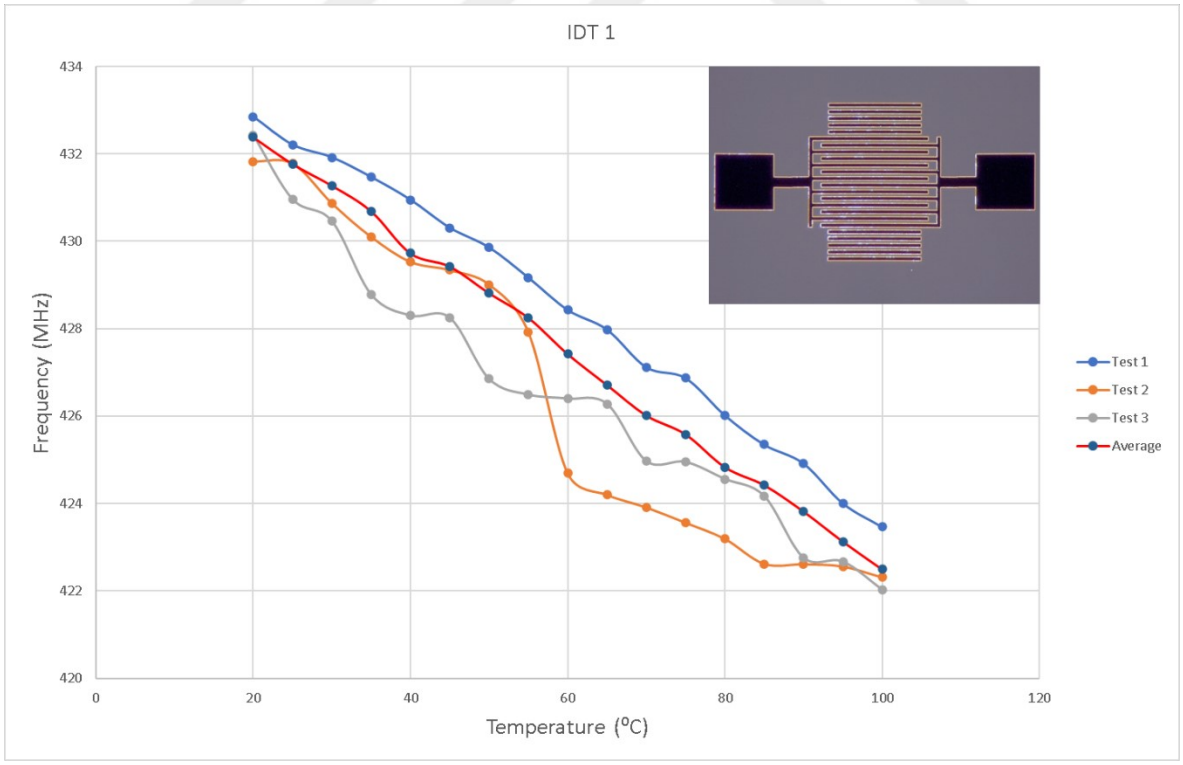

Figure 4.21. Temperature response of the fabricated IDT 1.

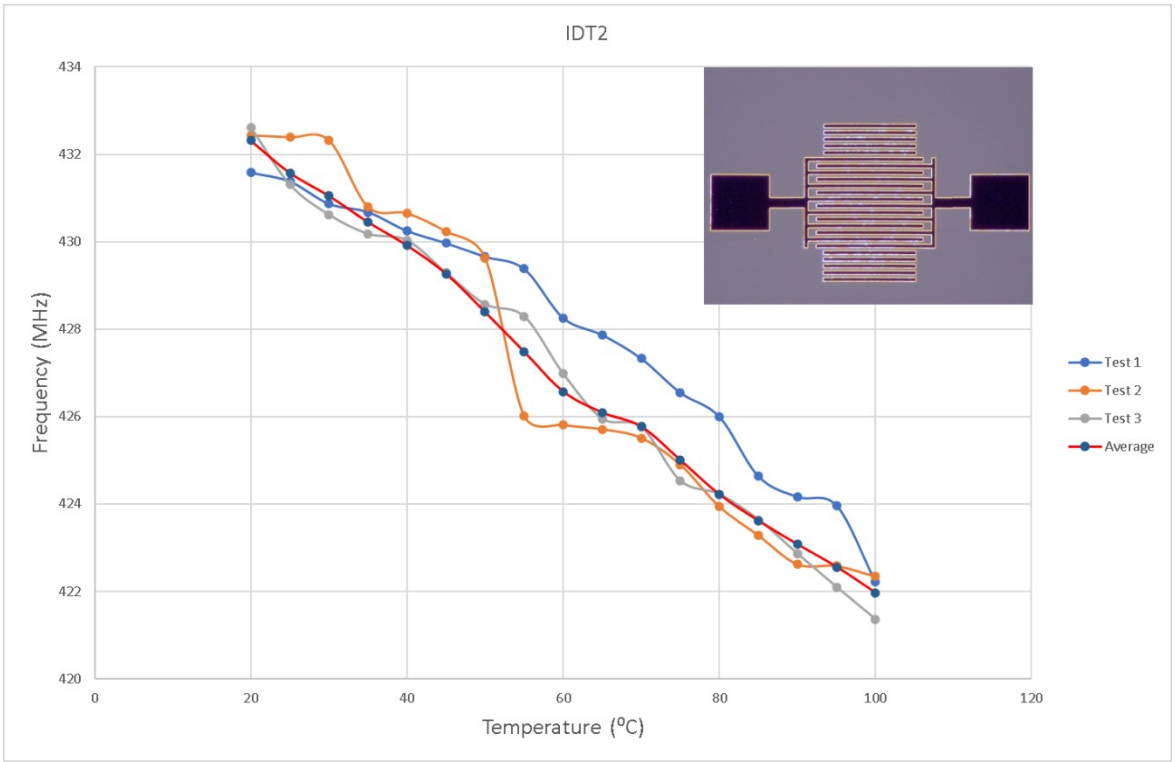

Figure 4.22. Temperature response of the fabricated IDT 2

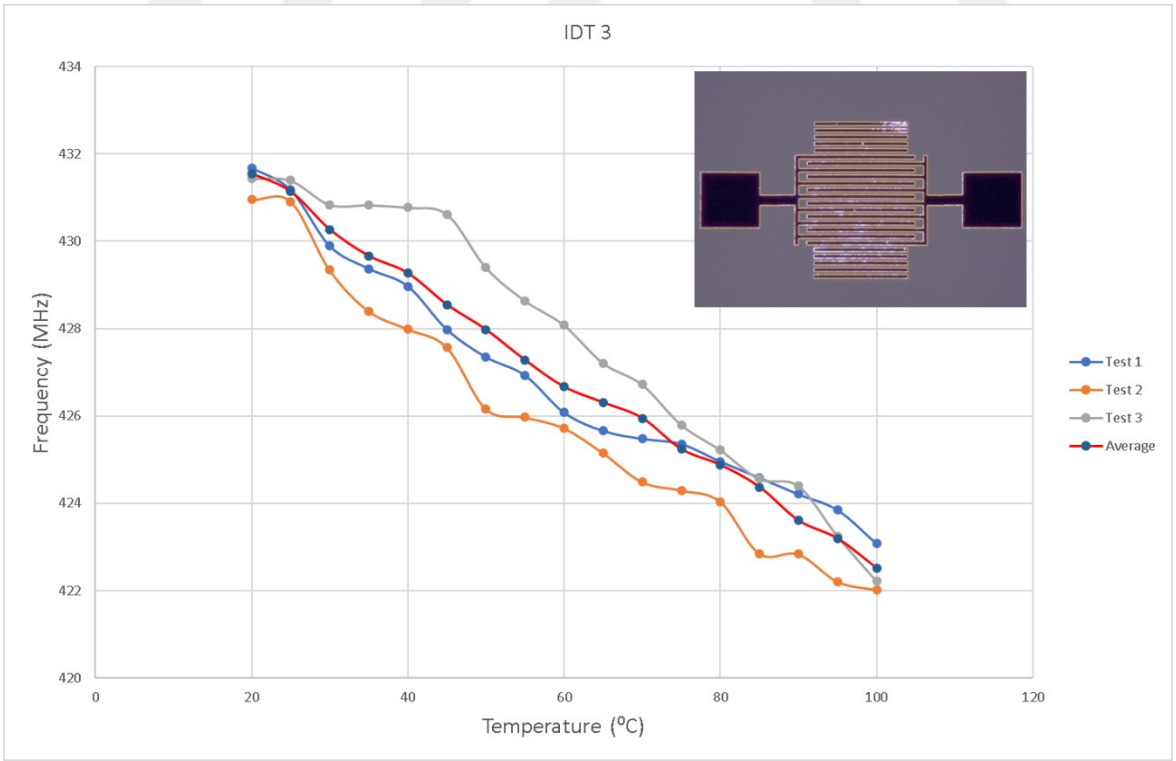

Figure 4.23. Temperature response of the fabricated IDT 3

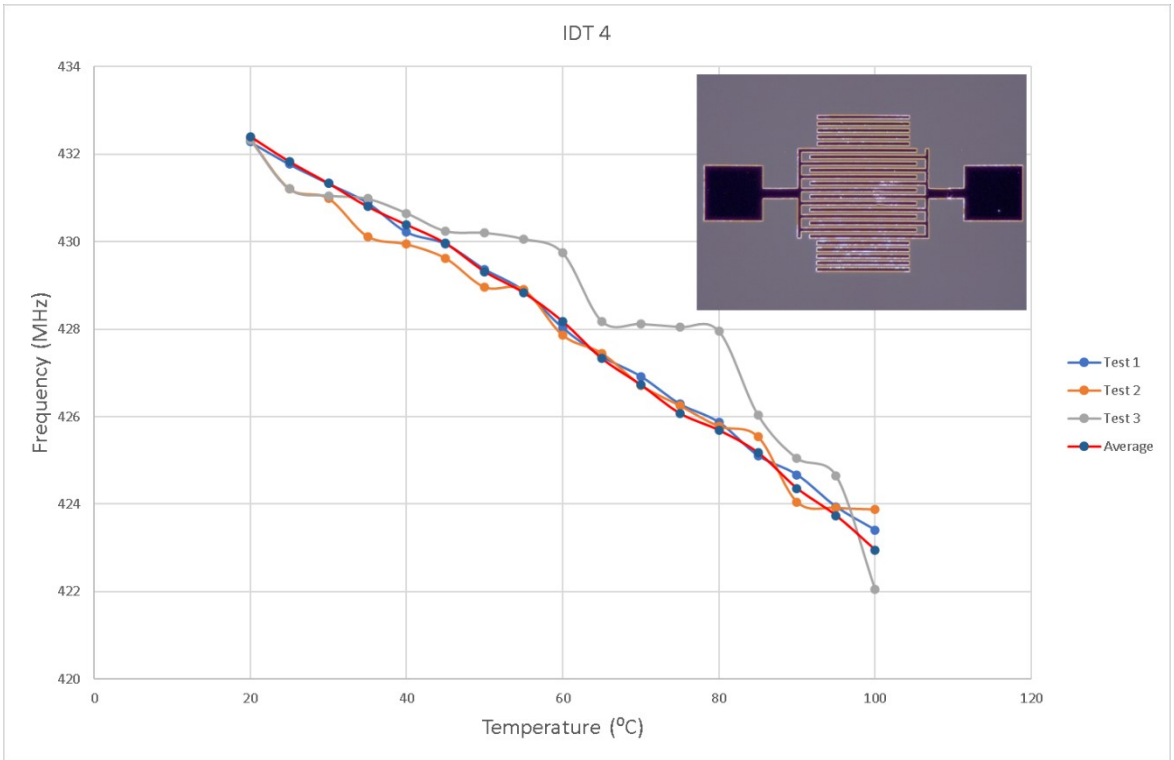

Figure 4.24. Temperature response of the fabricated IDT 4

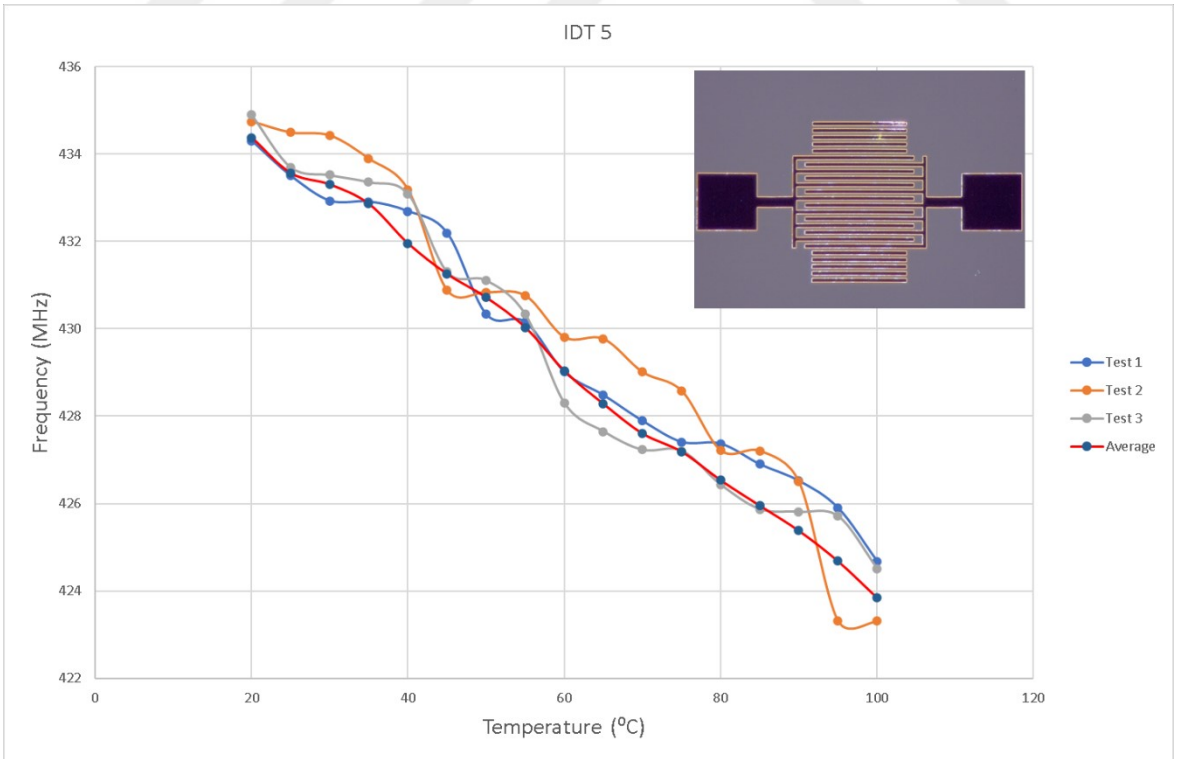

Figure 4.25. Temperature response of the fabricated IDT 5

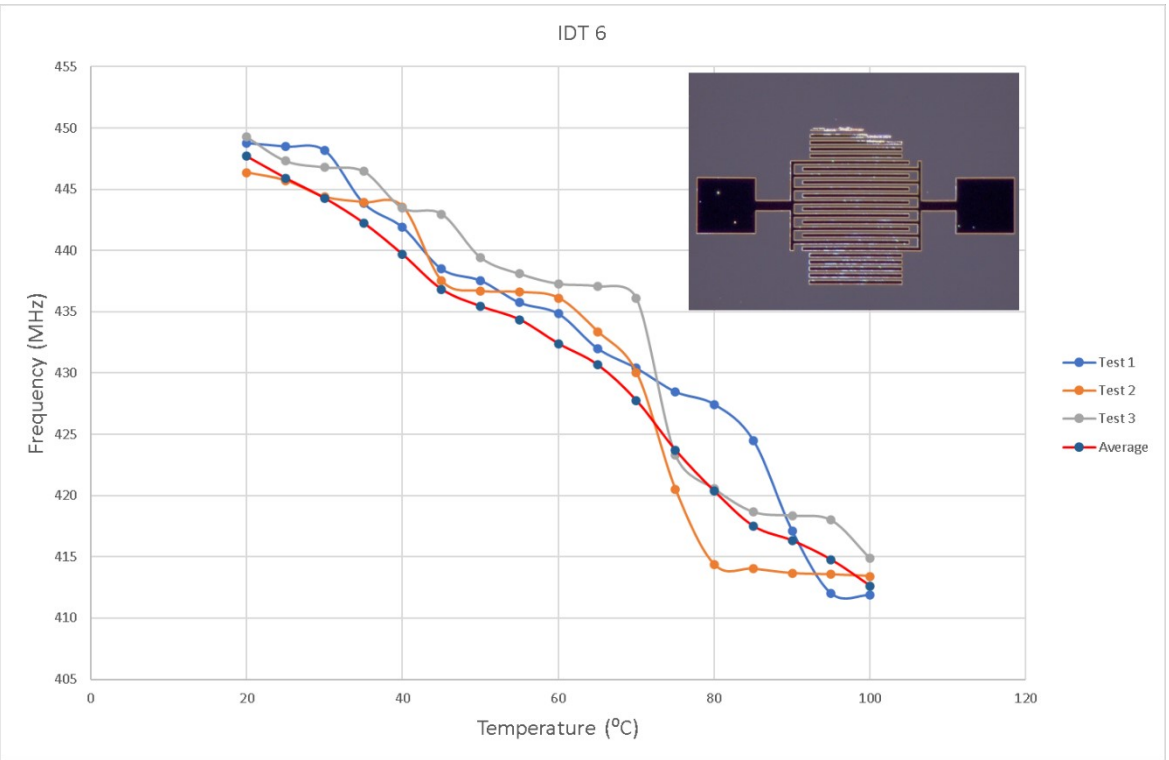

Figure 4.26. Temperature response of the fabricated IDT 6.

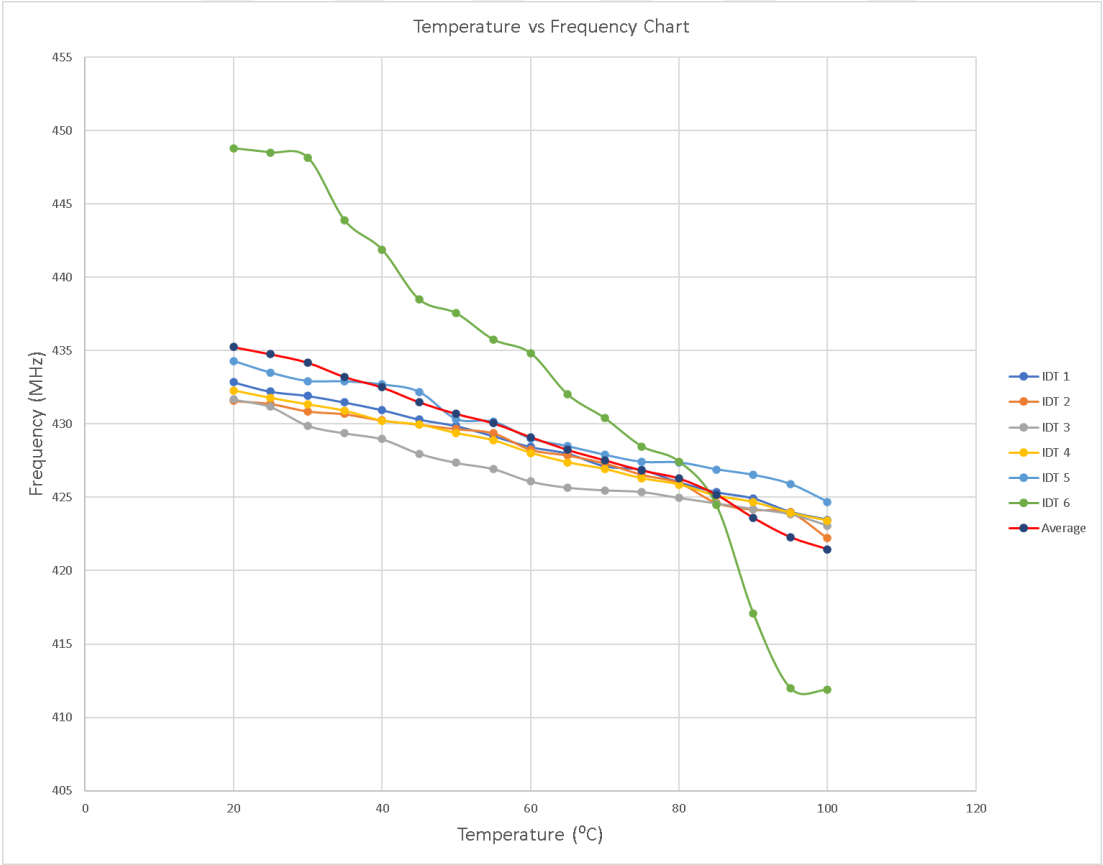

Figure 4.27. Temperature responses of all the IDT structures.

The fabricated IDT structures show very good linearity when tested against temperature. The average R2 values from 10 tests for each IDT structure along with the combined average value is illustrated in figure 4.28.

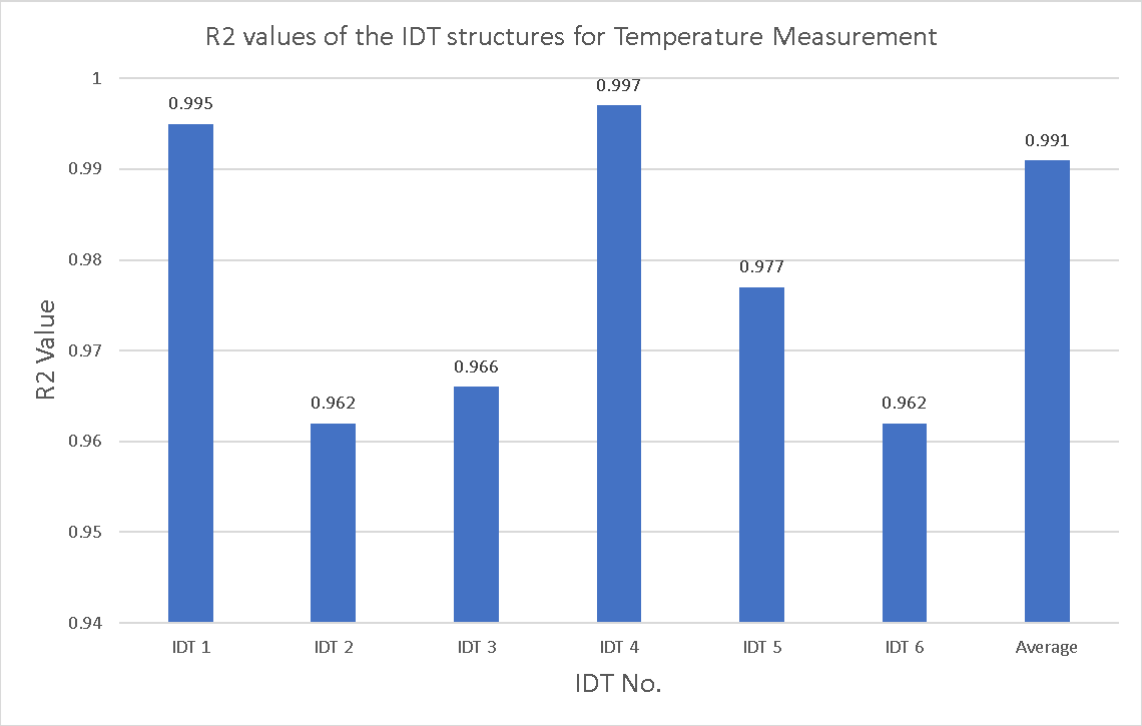

Figure 4.28. R2 values for the fabricated IDTs against temperature.

5 CONCLUSIONS

The main focus of this research was the fabrication of IDT structures using 3D printing technique in order to make the production process less time consuming and more efficient. To this end, 2PP based DLW printing technique was employed which enables maskless fabrication of the proposed IDT structures. The temperature response of the fabricated structure was also measured in this study.

CAD of the proposed IDT structures were also constructed using Siemens NX and klayout editor softwares. The generated files were utilized in the fabrication and also in the modelling optimization of the proposed IDT structures. Before realization of the fabrication, the IDT structures were optimization using FEA process using COMSOL. Their responses were studied and the final optimized design for the fabrication was selected using the results from the simulation.

Afterwards, the IDT structures were fabricated using Nanoscribe's Professional Photonic GT 3D printer using DLW printing technique. The SEM and electron microscope images of the fabricated IDT structures were taken and studied. The images showed consistency of the employed printing method with the proposed design.

The frequency response of the fabricated IDT structures were measured using a test setup and the peak frequency was found to be 426.2 MHz. The results from the simulation showed the resonant frequency to be 424.01 MHz. According to those result only 0.5% error were calculated between those two measurements. This error is well within the acceptable range.

Finally, the IDT structures were tested in a climatic test chamber for the response towards the changes in temperature. The preliminary results of those tests showed their response to be very much linear with the changes in temperature. The average R^2 value of all the responses was >0.9.

The following conclusion can be drawn from this research:

- The fabrication of micro, even nano, structures with great accuracy using 3D printing technique is feasible.

- The deployed of 3D printers for the fabrication of MEMS and NEMS device makes the fabrication process cheaper and less time consuming when compared to the conventional methods.
- Using DLW based 2PP printing techniques, it is possible to print highly conductive materials such as gold.
- The FEA analysis should be performed before the fabrication process in order to optimize the parameters. The use of different computer softwares for analysis shows consistency in results.
- A very good corelation between the simulation and experimental results are obtained which shows that computer can be used for the initial analysis.
- The experimental results obtained from 6 IDT structures shows a very good corelation, with the average R^2 value > 0.9.

Many future researches can be performed on the basis of this dissertation. Some suggestions for the possible future researches are stated below:

- Development and integration of the reader circuit for the direct reading of temperature.
- Modifying the design of the current IDT structures in order to measure other physical quantities, such as pressure, and gases, while employing 3D printing technologies for the fabrication.
- Testing of the IDT structure reader circuit's transmission range.

REFERENCES

1. Zhan, Z., An, J., Wei, Y., Tran, V. T., & Du, H. (2017). Inkjet-printed optoelectronics. *Nanoscale*, *9*(3), 965–993. https://doi.org/10.1039/C6NR08220C

2. Khan, Y., Thielens, A., Muin, S., Ting, J., Baumbauer, C., & Arias, A. C. (2020). A New Frontier of Printed Electronics: Flexible Hybrid Electronics. *Advanced Materials*, *32*(15), 1905279. https://doi.org/10.1002/adma.201905279

3. Khan, S., Lorenzelli, L., & Dahiya, R. S. (2015). Technologies for Printing Sensors and Electronics Over Large Flexible Substrates: A Review. *IEEE Sensors Journal*, *15*(6), 3164–3185. https://doi.org/10.1109/JSEN.2014.2375203

4. Mohammed, M. G., & Kramer, R. (2017). All-Printed Flexible and Stretchable Electronics. *Advanced Materials*, *29*(19), 1604965. https://doi.org/10.1002/adma.201604965

5. Au, A. K., Huynh, W., Horowitz, L. F., & Folch, A. (2016). 3D-Printed Microfluidics. *Angewandte Chemie International Edition*, *55*(12), 3862–3881. https://doi.org/10.1002/anie.201504382

6. Berggren, M., Nilsson, D., & Robinson, N. D. (2007). Organic materials for printed electronics. *Nature Materials*, *6*(1), 3–5. https://doi.org/10.1038/nmat1817

7. Perelaer, J., Smith, P. J., Mager, D., Soltman, D., Volkman, S. K., Subramanian, V., … Schubert, U. S. (2010). Printed electronics: the challenges involved in printing devices, interconnects, and contacts based on inorganic materials. *Journal of Materials Chemistry*, *20*(39), 8446. https://doi.org/10.1039/c0jm00264j

8. Pease, R. F., & Chou, S. Y. (2008). Lithography and Other Patterning Techniques for Future Electronics. *Proceedings of the IEEE*, *96*(2), 248–270. https://doi.org/10.1109/JPROC.2007.911853

9. Nathan, A., Ahnood, A., Cole, M. T., Sungsik Lee, Suzuki, Y., Hiralal, P., … Milne, W. I. (2012). Flexible Electronics: The Next Ubiquitous Platform. *Proceedings of the IEEE*, *100*(Special Centennial Issue), 1486–1517. https://doi.org/10.1109/JPROC.2012.2190168

10. Søndergaard, R. R., Hösel, M., & Krebs, F. C. (2013). Roll-to-Roll fabrication of large area functional organic materials. *Journal of Polymer Science Part B: Polymer Physics*, *51*(1), 16–34. https://doi.org/10.1002/polb.23192

11. Moscato, S., Bahr, R., Le, T., Pasian, M., Bozzi, M., Perregrini, L., & Tentzeris, M. M. (2015). Additive manufacturing of 3D substrate integrated waveguide components. *Electronics Letters*, *51*(18), 1426–1428. https://doi.org/10.1049/el.2015.2298

12. Hine Tong, D. lo, Manga, A. A., Minard, P., Delattre, A., Crowther-Alwyn, L., & Borel, P. (2016). Comparative study of WLAN dual-band monopole antennas printed and etched on paper and PET substrates. In *2016 46th European Microwave Conference (EuMC)* (pp. 1243–1246). IEEE. https://doi.org/10.1109/EuMC.2016.7824575

13. Morimoto, Y., Memarian, M., Li, X., & Itoh, T. (2017). Open-End Microstrip Line Terminations Using Lossy Gray-Scale Inkjet Printing. *IEEE Transactions on Microwave Theory and Techniques*, *65*(12), 4861–4870. https://doi.org/10.1109/TMTT.2017.2716352

14. Sahu, A., Aaen, P. H., Lewandowski, A., Shkunov, M., Rigas, G., Blanchard, P. T., … Devabhaktuni, V. K. (2017). Robust Microwave Characterization of Inkjet-Printed Coplanar Waveguides on Flexible Substrates. *IEEE Transactions on Instrumentation and Measurement*, *66*(12), 3271–3279. https://doi.org/10.1109/TIM.2017.2753384

15. Au, A. K., Lee, W., & Folch, A. (2014). Mail-order microfluidics: evaluation of stereolithography for the production of microfluidic devices. *Lab Chip*, *14*(7), 1294–1301. https://doi.org/10.1039/C3LC51360B

16. Adams, J. J., Slimmer, S. C., Lewis, J. A., & Bernhard, J. T. (2015). 3D-printed spherical dipole antenna integrated on small RF node. *Electronics Letters*, *51*(9), 661–662. https://doi.org/10.1049/el.2015.0256

17. Kimionis, J., Isakov, M., Koh, B. S., Georgiadis, A., & Tentzeris, M. M. (2015). 3D-Printed Origami Packaging With Inkjet-Printed Antennas for RF Harvesting

Sensors. *IEEE Transactions on Microwave Theory and Techniques*, *63*(12), 4521–4532. https://doi.org/10.1109/TMTT.2015.2494580

18. Rahman, M. T., Moser, R., Zbib, H. M., Ramana, C. v., & Panat, R. (2018). 3D printed high performance strain sensors for high temperature applications. *Journal of Applied Physics*, *123*(2), 024501. https://doi.org/10.1063/1.4999076

19. Zhang, D., Jiang, C., Tong, J., Zong, X., & Hu, W. (2018). Flexible Strain Sensor Based on Layer-by-Layer Self-Assembled Graphene/Polymer Nanocomposite Membrane and Its Sensing Properties. *Journal of Electronic Materials*, *47*(4), 2263–2270. https://doi.org/10.1007/s11664-017-6052-1

20. Ando, B., & Baglio, S. (2013). All-Inkjet Printed Strain Sensors. *IEEE Sensors Journal*, *13*(12), 4874–4879. https://doi.org/10.1109/JSEN.2013.2276271

21. Yang, H., Rahman, M. T., Du, D., Panat, R., & Lin, Y. (2016). 3-D printed adjustable microelectrode arrays for electrochemical sensing and biosensing. *Sensors and Actuators B: Chemical*, *230*, 600–606. https://doi.org/10.1016/j.snb.2016.02.113

22. Rahman, T., Renaud, L., Heo, D., Renn, M., & Panat, R. (2015). Aerosol based direct-write micro-additive fabrication method for sub-mm 3D metal-dielectric structures. *Journal of Micromechanics and Microengineering*, *25*(10), 107002. https://doi.org/10.1088/0960-1317/25/10/107002

23. Goth, C., Putzo, S., & Franke, J. (2011). Aerosol Jet printing on rapid prototyping materials for fine pitch electronic applications. In *2011 IEEE 61st Electronic Components and Technology Conference (ECTC)* (pp. 1211–1216). IEEE. https://doi.org/10.1109/ECTC.2011.5898664

24. Cho, J. H., Lee, J., Xia, Y., Kim, B., He, Y., Renn, M. J., … Daniel Frisbie, C. (2008). Printable ion-gel gate dielectrics for low-voltage polymer thin-film transistors on plastic. *Nature Materials*, *7*(11), 900–906. https://doi.org/10.1038/nmat2291

25. Mette, A., Richter, P. L., Hörteis, M., & Glunz, S. W. (2007). Metal aerosol jet printing for solar cell metallization. *Progress in Photovoltaics: Research and Applications*, *15*(7), 621–627. https://doi.org/10.1002/pip.759

26. Yang, C., Zhou, E., Miyanishi, S., Hashimoto, K., & Tajima, K. (2011). Preparation of Active Layers in Polymer Solar Cells by Aerosol Jet Printing. *ACS Applied Materials & Interfaces*, *3*(10), 4053–4058. https://doi.org/10.1021/am200907k

27. Ertugrul, I., & Waqar, T. (2020). Withdrawal Notice: Fabrication of Bidirectional Electrothermal Microactuator by Two-Photon Polymerization. *Current Nanoscience*, *16*. https://doi.org/10.2174/1573413716666201217123735

28. Ertugrul, I. (2020). The Fabrication of Micro Beam from Photopolymer by Digital Light Processing 3D Printing Technology. *Micromachines*, *11*(5), 518. https://doi.org/10.3390/mi11050518

29. Rayleigh, Lord. (1885). On Waves Propagated along the Plane Surface of an Elastic Solid. *Proceedings of the London Mathematical Society*, *s1-17*(1), 4–11. https://doi.org/10.1112/plms/s1-17.1.4

30. Kirschner, J. (2010). *Surface Acoustic Wave Sensors (SAWS) : Design for Application.*

31. Liu, B., Zhang, C., Ji, X., Chen, J., & Han, T. (2014). An Improved Performance Frequency Estimation Algorithm for Passive Wireless SAW Resonant Sensors. *Sensors*, *14*(12), 22261–22273. https://doi.org/10.3390/s141222261

32. Hartemann, P., & Dieulesaint, E. (1969). Intrinsic compensation of sidelobes in a dispersive acoustic delay line. *Electronics Letters*, *5*(10), 219–220. https://doi.org/10.1049/el:19690168

33. White, R. M., & Voltmer, F. W. (1965). DIRECT PIEZOELECTRIC COUPLING TO SURFACE ELASTIC WAVES. *Applied Physics Letters*, *7*(12), 314–316. https://doi.org/10.1063/1.1754276

34. Diaz, J. F., Karrer, H. E., Kusters, J. A., Matsinger, J. H., & Schulz, M. B. (1975). The Temperature Coefficient of Delay-Time for X-Propagating Acoustic Surface-Waves on Rotated Y-Cuts of Alpha Quartz. *IEEE Transactions on Sonics and Ultrasonics*, *22*(1), 46–49. https://doi.org/10.1109/T-SU.1975.30774

35. Sittig, E. K., & Coquin, G. A. (1968). Filters and Dispersive Delay Lines Using Repetitively Mismatched Ultrasonic Transmission Lines. *IEEE Transactions on*

Sonics and Ultrasonics, *15*(2), 111–118. https://doi.org/10.1109/T-SU.1968.29456

36. Smith, W. R., & Pedler, W. F. (1975). Fundamental- and Harmonic-Frequency Circuit-Model Analysis of Lnterdigital Transducers with Arbitralry Metallization Ratios and Polarity Sequences. *IEEE Transactions on Microwave Theory and Techniques*, *23*(11), 853–864. https://doi.org/10.1109/TMTT.1975.1128703

37. Smith, W. R., Gerard, H. M., Collins, J. H., Reeder, T. M., & Shaw, H. J. (1969). Analysis of Interdigital Surface Wave Transducers by Use of an Equivalent Circuit Model. *IEEE Transactions on Microwave Theory and Techniques*, *17*(11), 856–864. https://doi.org/10.1109/TMTT.1969.1127075

38. Tancrell, R. H., & Holland, M. G. (1971). Acoustic surface wave filters. *Proceedings of the IEEE*, *59*(3), 393–409. https://doi.org/10.1109/PROC.1971.8180

39. Hartmann, C. S., Bell, D. T., & Rosenfeld, R. C. (1973). Impulse Model Design of Acoustic Surface-Wave Filters. *IEEE Transactions on Microwave Theory and Techniques*, *21*(4), 162–175. https://doi.org/10.1109/TMTT.1973.1127967

40. Tobolka, G. (1979). Mixed Matrix Representation of SAW Transducers. *IEEE Transactions on Sonics and Ultrasonics*, *26*(6), 426–427. https://doi.org/10.1109/T-SU.1979.31128

41. Wright, P. V. (n.d.). A new generalized modeling of SAW transducers and gratings. In *Proceedings of the 43rd Annual Symposium on Frequency Control* (pp. 596–605). IEEE. https://doi.org/10.1109/FREQ.1989.68920

42. Ro, R., Tung, H.-Y., & Wu, S.-J. (2004). Design of Two-Track Surface Acoustic Wave Filters with Width-Controlled Reflectors. *Japanese Journal of Applied Physics*, *43*(2), 688–694. https://doi.org/10.1143/JJAP.43.688

43. Achour, B., Aloui, N., Fourati, N., Zerrouki, C., & Yaakoubi, N. (2018). Modelling and simulation of SAW delay line sensors with COMSOL Multiphysics. In *Proceedings of MOL2NET 2018, International Conference on Multidisciplinary Sciences, 4th edition* (p. 5887). Basel, Switzerland: MDPI. https://doi.org/10.3390/mol2net-04-05887

44. el Gowini, M., & Moussa, W. (2009). A Reduced Three Dimensional Model for SAW Sensors Using Finite Element Analysis. *Sensors*, *9*(12), 9945–9964. https://doi.org/10.3390/s91209945

45. Elsherbini, M. M., Elkordy, M. F., & Gomaa, A. M. (2016). Using COMSOL to model high frequency surface acoustic wave (SAW) device. *Journal of Electrical and Electronics Engineering Research*, *8*(1), 1–8.

46. Krishnamurthy, S. (2007). *Wireless Passive Surface Acoustic Wave (SAW) Sensing System*.

47. Humphries, J., Figuroa, J., Gallagher, M., Gallagher, D., Weeks, A., & Malocha, D. (2016). *Interrogating Passive, Wireless SAW Sensors with the USRP B200mini*.

48. Malocha, D. C., Puccio, D., & Gallagher, D. (n.d.). Orthogonal frequency coding for SAW device applications. In *IEEE Ultrasonics Symposium, 2004* (pp. 1082–1085). IEEE. https://doi.org/10.1109/ULTSYM.2004.1417965

49. Reindl, L., Shrena, I., Kenshil, S., & Peter, R. (n.d.). Wireless measurement of temperature using surface acoustic waves sensors. In *IEEE International Frequency Control Sympposium and PDA Exhibition Jointly with the 17th European Frequency and Time Forum, 2003. Proceedings of the 2003* (pp. 935–941). IEEE. https://doi.org/10.1109/FREQ.2003.1275216

50. Binder, A., Bruckner, G., Schobernig, N., & Schmitt, D. (2013). Wireless Surface Acoustic Wave Pressure and Temperature Sensor With Unique Identification Based on ${\rm LiNbO}_{3}$. *IEEE Sensors Journal*, *13*(5), 1801–1805. https://doi.org/10.1109/JSEN.2013.2241052

51. Stoney, R., Donohoe, B., Geraghty, D., & O'Donnell, G. E. (2012). The Development of Surface Acoustic Wave Sensors (SAWs) for Process Monitoring. *Procedia CIRP*, *1*, 569–574. https://doi.org/10.1016/j.procir.2012.05.001

52. Ji, X., Fan, Y., Qi, H., Chen, J., Han, T., & Cai, P. (2014). A wireless demodulation system for passive surface acoustic wave torque sensor. *Review of Scientific Instruments*, *85*(12), 125001. https://doi.org/10.1063/1.4902180

53. Devkota, J., Ohodnicki, P., & Greve, D. (2017). SAW Sensors for Chemical Vapors and Gases. *Sensors*, *17*(4), 801. https://doi.org/10.3390/s17040801

54. Länge, K., Rapp, B. E., & Rapp, M. (2008). Surface acoustic wave biosensors: a review. *Analytical and Bioanalytical Chemistry*, *391*(5), 1509–1519. https://doi.org/10.1007/s00216-008-1911-5

55. Drafts, B. (2000). Acoustic Wave Technology Sensors. *https://www.fierceelectronics.com/components/acoustic-wave-technology-sensors*.

56. Malocha, D. C. (n.d.). Evolution of the SAW transducer for communication systems. In *IEEE Ultrasonics Symposium, 2004* (pp. 302–310). IEEE. https://doi.org/10.1109/ULTSYM.2004.1417726

57. Xu, S., Li, C., Li, H., Li, M., Qu, C., & Yang, B. (2015). Carbon dioxide sensors based on a surface acoustic wave device with a graphene–nickel– <scp>l</scp> -alanine multilayer film. *Journal of Materials Chemistry C*, *3*(16), 3882–3890. https://doi.org/10.1039/C4TC02986K

58. Malocha, D., Gallagher, M., Fisher, B., Humphries, J., Gallagher, D., & Kozlovski, N. (2013). A Passive Wireless Multi-Sensor SAW Technology Device and System Perspectives. *Sensors*, *13*(5), 5897–5922. https://doi.org/10.3390/s130505897

59. Seo, S.-H., Shin, W.-C., & Park, J.-S. (2002). A novel method of fabricating ZnO/diamond/Si multilayers for surface acoustic wave (SAW) device applications. *Thin Solid Films*, *416*(1–2), 190–196. https://doi.org/10.1016/S0040-6090(02)00725-3

60. Zakaria, M. R., Farhi Shamsuddin, M. A., Hashim, U., Adam, T., & Al-Mufti, A. W. (2014). Design and Fabrication of IDT Surface Acoustic Wave Device for Biosensor Application. In *2014 5th International Conference on Intelligent Systems, Modelling and Simulation* (pp. 760–764). IEEE. https://doi.org/10.1109/ISMS.2014.139

61. Maiwald, M., Werner, C., Zoellmer, V., & Busse, M. (2010). INKtelligent printed strain gauges. *Sensors and Actuators A: Physical*, *162*(2), 198–201. https://doi.org/10.1016/j.sna.2010.02.019

62. Thompson, B., & Yoon, H.-S. (2012). Aerosol printed carbon nanotube strain sensor. In T. E. Matikas (Ed.), (p. 83461C). https://doi.org/10.1117/12.914964

63. Zhang, Y., Anderson, N., Bland, S., Nutt, S., Jursich, G., & Joshi, S. (2017). All-printed strain sensors: Building blocks of the aircraft structural health monitoring system. *Sensors and Actuators A: Physical*, *253*, 165–172. https://doi.org/10.1016/j.sna.2016.10.007

64. Thompson, B., & Yoon, H.-S. (2013). Aerosol-Printed Strain Sensor Using PEDOT:PSS. *IEEE Sensors Journal*, *13*(11), 4256–4263. https://doi.org/10.1109/JSEN.2013.2264482

65. Wilson, W. C., & Atkinson, G. M. (2014). Passive Wireless Sensor Applications for NASA's Extreme Aeronautical Environments. *IEEE Sensors Journal*, *14*(11), 3745–3753. https://doi.org/10.1109/JSEN.2014.2322959

66. Romanosky, R. R., & Maley, S. M. (2013). Harsh environment sensor development for advanced energy systems. In T. George, M. S. Islam, & A. K. Dutta (Eds.), (p. 87250H). https://doi.org/10.1117/12.2015865

67. Fichtel, E., & Mcdaniel, A. (1994). *High temperature strain gage technology for gas turbine engines*.

68. Lei, J.-F., & Will, H. A. (1998). Thin-film thermocouples and strain-gauge technologies for engine applications. *Sensors and Actuators A: Physical*, *65*(2–3), 187–193. https://doi.org/10.1016/S0924-4247(97)01683-X

69. Watson, J., & Castro, G. (2015). A review of high-temperature electronics technology and applications. *Journal of Materials Science: Materials in Electronics*, *26*(12), 9226–9235. https://doi.org/10.1007/s10854-015-3459-4

70. Curie, J., & Curie, P. (1880). Développement par compression de l'électricité polaire dans les cristaux hémièdres à faces inclinées. *Bulletin de la Société minéralogique de France*, *3*(4), 90–93. https://doi.org/10.3406/bulmi.1880.1564

71. Madou, M. J. (2018). *Fundamentals of Microfabrication*. CRC Press. https://doi.org/10.1201/9781482274004

72. T., A. E. H. (1911). (1) Lehrbuch der Kristallphysik (mit Ausschluss der Kristalloptik) (2) Leçons de Cristallographie (3) Die Kristallgruppen nebst ihren Beziehungen zu den Raumgittern. *Nature*, *86*(2173), 544–546. https://doi.org/10.1038/086544a0

73. Cady, W. G. (1964). *Piezoelectricity: An Introduction To The Theory And Applications Of Electromechanical Phenomena In Crystals* (2nd Ed.). New York: McGraw-Hill Book Company, Inc.

74. Duran, P., & Moure, C. (1986). Piezoelectric ceramics. *Materials Chemistry and Physics*, *15*(3–4), 193–211. https://doi.org/10.1016/0254-0584(86)90001-5

75. Warren P., M. (1942). *Electromechanical Transducers And Wave Filters*. New York: D. Van Nostrand Company, Inc.

76. Gautschi, G. (2002). *Piezoelectric Sensorics*. Berlin, Heidelberg: Springer Berlin Heidelberg. https://doi.org/10.1007/978-3-662-04732-3

77. Rogacheva, N. N. (2020). *The Theory of Piezoelectric Shells and Plates*. CRC Press. https://doi.org/10.1201/9781003068129

78. Ikeda, T. (1996). *Fundamentals of Piezoelectricity*. Oxford Science Publications.

79. IEEE Standard on Piezoelectricity. (1988). *ANSI/IEEE Std*, 176–1987.

80. Publication and Proposed Revision of ANSI/IEEE Standard 176-1987 "ANSI/IEEE Standard on Piezoelectricity." (1996). *IEEE Transactions on Ultrasonics, Ferroelectrics and Frequency Control*, *43*(5), 717. https://doi.org/10.1109/TUFFC.1996.535477

81. Uchino, K. (2017). The Development of Piezoelectric Materials and the New Perspective. In *Advanced Piezoelectric Materials* (pp. 1–92). Elsevier. https://doi.org/10.1016/B978-0-08-102135-4.00001-1

82. Nuffer, J., & Bein, T. (2006). APPLICATION OF PIEZOELECTRIC MATERIALS IN TRANSPORTATION INDUSTRY.

83. ZHOU, J., SUN, H., & LIU, J. (2009). Application of Piezoelectric Ceramic Materials on Display Technology. *Bulletin of the Chinese Ceramic Society*.

84. Yeh, C.-H., Su, F.-C., Shan, Y.-S., Dosaev, M., Selyutskiy, Y., Goryacheva, I., & Ju, M.-S. (2020). Application of piezoelectric actuator to simplified haptic feedback system. *Sensors and Actuators A: Physical*, *303*, 111820. https://doi.org/10.1016/j.sna.2019.111820

85. Manbachi, A., & Cobbold, R. S. C. (2011). Development and Application of Piezoelectric Materials for Ultrasound Generation and Detection. *Ultrasound*, *19*(4), 187–196. https://doi.org/10.1258/ult.2011.011027

86. Giurgiutiu, V., Lin, B., Santoni-Bottai, G., & Cuc, A. (2011). Space Application of Piezoelectric Wafer Active Sensors for Structural Health Monitoring. *Journal of Intelligent Material Systems and Structures*, *22*(12), 1359–1370. https://doi.org/10.1177/1045389X11416029

87. Tingley, R. (2013). Method and application of piezoelectric energy harvesting as a mobile power source.

88. Campbell, C. (1998). *Surface Acoustic Wave Devices for Mobile and Wireless Communications*. San Diego: Academic Press.

89. Auld, B. A., & Green, R. E. (1974). Acoustic Fields and Waves in Solids: Two Volumes. *Physics Today*, *27*(10), 63–64. https://doi.org/10.1063/1.3128926

90. Morgan, D. P. (1985). Surface-Wave Devices for Signal Processing. *Elsevier*.

91. FARNELL, G. W. (1970). Properties of Elastic Surface Waves (pp. 109–166). https://doi.org/10.1016/B978-0-12-395666-8.50017-8

92. Haldar, S. K. (2018). *Mineral Exploration*. Elsevier. https://doi.org/10.1016/C2017-0-00902-3

93. Morgan, D. P. (n.d.). History of SAW devices. In *Proceedings of the 1998 IEEE International Frequency Control Symposium (Cat. No.98CH36165)* (pp. 439–460). IEEE. https://doi.org/10.1109/FREQ.1998.717937

94. Jones, S. (2010). *Ground vibration from underground railways: how simplifying assumptions limit prediction accuracy*.

95. He, H., Yang, J., Kosinski, J. A., & Wang, J. (2013). Thickness-shear vibration of a rectangular quartz plate with partial electrodes. *Acta Mechanica Solida Sinica*, *26*(2), 121–128. https://doi.org/10.1016/S0894-9166(13)60012-9

96. Campbell, J. J., & Jones, W. R. (1968). A method for estimating optimal crystal cuts and propagation directions for excitation of piezoelectric surface waves. *IEEE*

Transactions on Sonics and Ultrasonics, *15*(4), 209–217. https://doi.org/10.1109/T-SU.1968.29477

97. Slobodnik, A. J., Conway, E. D., & Delmonico, R. T. (1974). Microwave Acoustics Handbook, Vol. 1A, Surface Wave Velocities. *The Journal of the Acoustical Society of America*, *56*(4), 1307–1308. https://doi.org/10.1121/1.1903432

98. Malischewsky, P. G., & Tuan, T. T. (2009). A special relation between Young's modulus, Rayleigh-wave velocity, and Poisson's ratio. *The Journal of the Acoustical Society of America*, *126*(6), 2851–2853. https://doi.org/10.1121/1.3243464

99. Michel, B. (1992). Freund, L. B., Dynamic Fracture Mechanics. Cambridge etc., Cambridge University Press 1990. XVII, 563 pp., L 40.00 H/b. ISBN 0-521-30330-3 (Cambridge Monographs on Mechanics and Applied Mathematics). *ZAMM - Journal of Applied Mathematics and Mechanics / Zeitschrift für Angewandte Mathematik und Mechanik*, *72*(8), 383–384. https://doi.org/10.1002/zamm.19920720818

100. Lipiński, M. J., Wdowska, M. K., & Jaroń, Ł. (2017). Shear Wave Velocity for Evaluation of State of Cohesionless Soils with Fines. *IOP Conference Series: Materials Science and Engineering*, *245*, 032083. https://doi.org/10.1088/1757-899X/245/3/032083

101. Yang, W. (2014). Elastic Waves in a Perfect Elastic Solid. In *Reflection Seismology* (pp. 19–46). Elsevier. https://doi.org/10.1016/B978-0-12-409538-0.00002-6

102. Chin, M. L. (2006). *A fabrication study of surface acoustic wave devices for magnetic field detection*.

103. Connacher, W., Zhang, N., Huang, A., Mei, J., Zhang, S., Gopesh, T., & Friend, J. (2018). Micro/nano acoustofluidics: materials, phenomena, design, devices, and applications. *Lab on a Chip*, *18*(14), 1952–1996. https://doi.org/10.1039/C8LC00112J

104. Ding, X., Li, P., Lin, S.-C. S., Stratton, Z. S., Nama, N., Guo, F., … Huang, T. J. (2013). Surface acoustic wave microfluidics. *Lab on a Chip*, *13*(18), 3626. https://doi.org/10.1039/c3lc50361e

105. Dong-Pei Chen, & Haus, H. A. (1985). Analysis of Metal-Strip SAW Gratings and Transducers. *IEEE Transactions on Sonics and Ultrasonics*, *32*(3), 395–408. https://doi.org/10.1109/T-SU.1985.31609

106. Hartmann, C. S., Wright, P. V., Kansy, R. J., & Garber, E. M. (1982). An Analysis of SAW Interdigital Transducers with Internal Reflections and the Application to the Design of Single-Phase Unidirectional Transducers. In *1982 Ultrasonics Symposium* (pp. 40–45). IEEE. https://doi.org/10.1109/ULTSYM.1982.197784

107. Mamishev, A. V., Sundara-Rajan, K., Fumin Yang, Yanqing Du, & Zahn, M. (2004). Interdigital sensors and transducers. *Proceedings of the IEEE*, *92*(5), 808–845. https://doi.org/10.1109/JPROC.2004.826603

108. Rathod, V. T. (2019). A Review of Electric Impedance Matching Techniques for Piezoelectric Sensors, Actuators and Transducers. *Electronics*, *8*(2), 169. https://doi.org/10.3390/electronics8020169

109. Wang, W., & He, S. (2008). A Love Wave Reflective Delay Line with Polymer Guiding Layer for Wireless Sensor Application. *Sensors*, *8*(12), 7917–7929. https://doi.org/10.3390/s8127917

110. Tanski, W. J. (1979). Surface Acoustic Wave Resonators on Quartz. *IEEE Transactions on Sonics and Ultrasonics*, *26*(2), 93–104. https://doi.org/10.1109/T-SU.1979.31073

111. Huang, F., Paige, E. G. S., & Selviah, D. R. (1985). The 180 Degree Reflectivity and Velocity Perturbation of Thin Metal Dots. In *IEEE 1985 Ultrasonics Symposium* (pp. 11–15). IEEE. https://doi.org/10.1109/ULTSYM.1985.198469

112. McCormack, B., Geraghty, D., & O'Mahony, M. (2011). Modeling of surface acoustic wave strain sensors using coupling-of-modes analysis. *IEEE Transactions on Ultrasonics, Ferroelectrics, and Frequency Control*, *58*(11), 2461–2468. https://doi.org/10.1109/TUFFC.2011.2102

113. Ash, E. A. (1970). Surface Wave Grating Reflectors and Resonators. In *G-MTT 1970 International Microwave Symposium* (pp. 385–386). IEEE. https://doi.org/10.1109/GMTT.1970.1122853

114. Bell, D. L. T., & Li, R. C. M. (1976). Surface-acoustic-wave resonators. *Proceedings of the IEEE*, *64*(5), 711–721. https://doi.org/10.1109/PROC.1976.10200

115. Wright, P. V. (n.d.). A review of SAW resonator filter technology. In *IEEE 1992 Ultrasonics Symposium Proceedings* (pp. 29–38). IEEE. https://doi.org/10.1109/ULTSYM.1992.276068

116. Reindl, L., Scholl, G., Ostertag, T., Scherr, H., Wolff, U., & Schmidt, F. (1998). Theory and application of passive SAW radio transponders as sensors. *IEEE Transactions on Ultrasonics, Ferroelectrics and Frequency Control*, *45*(5), 1281–1292. https://doi.org/10.1109/58.726455

117. Reindl, L., Scholl, G., Ostertag, T., Ruppel, C. C. W., Bulst, W.-E., & Seifert, F. (n.d.). SAW devices as wireless passive sensors. In *1996 IEEE Ultrasonics Symposium. Proceedings* (pp. 363–367). IEEE. https://doi.org/10.1109/ULTSYM.1996.583993

118. Augustine, R., Sarry, F., Kalarikkal, N., Thomas, S., Badie, L., & Rouxel, D. (2016). Surface Acoustic Wave Device with Reduced Insertion Loss by Electrospinning P(VDF–TrFE)/ZnO Nanocomposites. *Nano-Micro Letters*, *8*(3), 282–290. https://doi.org/10.1007/s40820-016-0088-2

119. Soluch, W. (n.d.). Scattering matrix approach to one port SAW resonators. In *Proceedings of the 1999 Joint Meeting of the European Frequency and Time Forum and the IEEE International Frequency Control Symposium (Cat. No.99CH36313)* (pp. 859–862). IEEE. https://doi.org/10.1109/FREQ.1999.841440

120. Ricco, A. J., Martin, S. J., & Zipperian, T. E. (1985). Surface acoustic wave gas sensor based on film conductivity changes. *Sensors and Actuators*, *8*(4), 319–333. https://doi.org/10.1016/0250-6874(85)80031-7

121. Grate, J. W., Rose-Pehrsson, S. L., Venezky, D. L., Klusty, Mark., & Wohltjen, Hank. (1993). Smart sensor system for trace organophosphorus and organosulfur vapor detection employing a temperature-controlled array of surface acoustic wave sensors, automated sample preconcentration, and pattern recognition. *Analytical Chemistry*, *65*(14), 1868–1881. https://doi.org/10.1021/ac00062a011

122. Hivert, B., Hoummady, M., Henrioud, J. M., & Hauden, D. (1994). Feasibility of surface acoustic wave (SAW) sensor array processing with formal neural networks. *Sensors and Actuators B: Chemical*, *19*(1–3), 645–648. https://doi.org/10.1016/0925-4005(93)01113-I

123. Bandat, P. A., Wlodarskit, W., & Pisarkiewicz, T. (n.d.). Theory, Design And Operation Of A Conductivity Based Surface Acoustic Wave Ozone Sensor. In *Proceedings of the International Solid-State Sensors and Actuators Conference - TRANSDUCERS '95* (pp. 755–757). IEEE. https://doi.org/10.1109/SENSOR.1995.721942

124. D'Amico, A., & Verona, E. (1989). Saw sensors. *Sensors and Actuators*, *17*(1–2), 55–66. https://doi.org/10.1016/0250-6874(89)80064-2

125. Ballantine, D. S., & Wohltjen, H. (1989). Surface acoustic wave devices for chemical analysis. *Analytical Chemistry*, *61*(11), 704A-715A. https://doi.org/10.1021/ac00186a001

126. Kavalov, D., & Kalinin, V. (2002). Neural network surface acoustic wave RF signal processor for digital modulation recognition. *IEEE Transactions on Ultrasonics, Ferroelectrics and Frequency Control*, *49*(9), 1280–1290. https://doi.org/10.1109/TUFFC.2002.1041545

127. McAlernon, P., Slater, J. M., Lowthian, P., & Appleton, M. (1996). Interpreting signals from an array of non-specific piezoelectric chemical sensors. *The Analyst*, *121*(6), 743. https://doi.org/10.1039/an9962100743

128. Natale, C. di, Davide, F. A. M., & D'Amico, A. (1995). A self-organizing system for pattern classification: time varying statistics and sensor drift effects. *Sensors and Actuators B: Chemical*, *27*(1–3), 237–241. https://doi.org/10.1016/0925-4005(94)01593-7

129. Hivert, B., Hoummady, M., Mielle, P., Mauvais, G., Henrioud, J. M., & Hauden, D. (1995). A fast and reproducible method for gas sensor screening to flavour compounds. *Sensors and Actuators B: Chemical*, *27*(1–3), 242–245. https://doi.org/10.1016/0925-4005(94)01594-8

130. Davide, F. A. M., & D'Amico, A. (1992). Pattern recognition from sensor arrays: Theoretical considerations. *Sensors and Actuators A: Physical*, *32*(1–3), 507–518. https://doi.org/10.1016/0924-4247(92)80036-3

131. Hoummady, M., Campitelli, A., & Wlodarski, W. (1997). Acoustic wave sensors: design, sensing mechanisms and applications. *Smart Materials and Structures*, *6*(6), 647–657. https://doi.org/10.1088/0964-1726/6/6/001

132. Puccio, D., Malocha, D. C., Gallagher, D., & Hines, J. (n.d.). SAW sensors using orthogonal frequency coding. In *Proceedings of the 2004 IEEE International Frequency Control Symposium and Exposition, 2004.* (pp. 307–310). IEEE. https://doi.org/10.1109/FREQ.2004.1418470

133. Hauden, D., Jaillet, G., & Coquerel, R. (1981). Temperature Sensor Using SAW Delay Line. In *1981 Ultrasonics Symposium* (pp. 148–151). IEEE. https://doi.org/10.1109/ULTSYM.1981.197598

134. Bao, X. Q., Burkhard, W., Varadan, V. V., & Varadan, V. K. (1987). SAW Temperature Sensor and Remote Reading System. In *IEEE 1987 Ultrasonics Symposium* (pp. 583–586). IEEE. https://doi.org/10.1109/ULTSYM.1987.199024

135. Tirole, N., Choujaa, A., Hauden, D., Martin, G., Blind, P., & Froelicher, M. (1993). Lamb waves pressure sensor using an AlN/Si structure. In *1993 Proceedings IEEE Ultrasonics Symposium* (pp. 371–374 vol.1). IEEE. https://doi.org/10.1109/ULTSYM.1993.339466

136. Vlassov, Yu. N., Kozlov, A. S., Pashchin, N. S., & Yakovkin, I. D. (n.d.). Precision SAW pressure sensors. In *1993 IEEE International Frequency Control Symposium* (pp. 665–669). IEEE. https://doi.org/10.1109/FREQ.1993.367460

137. Schimetta, G., Dollinger, F., Scholl, G., & Weigel, R. (n.d.). Wireless pressure and temperature measurement using a SAW hybrid sensor. In *2000 IEEE Ultrasonics*

Symposium. Proceedings. An International Symposium (Cat. No.00CH37121) (pp. 445–448). IEEE. https://doi.org/10.1109/ULTSYM.2000.922590

138. A. Talbi, F. S. (n.d.). Development of SAW pressure sensor using ZnO/Si structure. In *Proceedings of the 2004 IEEE International Frequency Control Symposium and Exposition, 2004.* (pp. 566–570). IEEE. https://doi.org/10.1109/FREQ.2004.1418521

139. Buff, W., Rusko, M., Vandahl, T., Goroll, M., & Moller, F. (n.d.). A differential measurement SAW device for passive remote sensoring. In *1996 IEEE Ultrasonics Symposium. Proceedings* (pp. 343–346). IEEE. https://doi.org/10.1109/ULTSYM.1996.583988

140. Josse, F., Haworth, D. T., Kelkar, U. R., & Shana, Z. A. (1990). LiNbO3 acoustic plate mode sensor for dilute ionic solutions. *Electronics Letters*, *26*(13), 834. https://doi.org/10.1049/el:19900547

141. Campitelli, A. P., Wlodarski, W., & Hoummady, M. (1998). Identification of natural spring water using shear horizontal SAW based sensors. *Sensors and Actuators B: Chemical*, *49*(3), 195–201. https://doi.org/10.1016/S0925-4005(98)00120-8

142. Kovacs, G., Lubking, G. W., Vellekoop, M. J., & Venema, A. (n.d.). Love waves for (bio)-chemical sensing in liquids. In *IEEE 1992 Ultrasonics Symposium Proceedings* (pp. 281–285). IEEE. https://doi.org/10.1109/ULTSYM.1992.275995

143. Gizeli, E., Goddard, N. J., Lowe, C. R., & Stevenson, A. C. (1992). A Love plate biosensor utilising a polymer layer. *Sensors and Actuators B: Chemical*, *6*(1–3), 131–137. https://doi.org/10.1016/0925-4005(92)80044-X

144. Kovacs, G., Vellekoop, M. J., Haueis, R., Lubking, G. W., & Venema, A. (1994). A love wave sensor for (bio)chemical sensing in liquids. *Sensors and Actuators A: Physical*, *43*(1–3), 38–43. https://doi.org/10.1016/0924-4247(93)00660-V

145. Grate, J. W., Martin, S. J., & White, R. M. (1993). Acoustic Wave Microsensors. *Analytical Chemistry*, *65*(21), 940A-948A. https://doi.org/10.1021/ac00069a728

146. Ye, X., Fang, L., Liang, B., Wang, Q., Wang, X., He, L., … Ko, W. H. (2011). Studies of a high-sensitive surface acoustic wave sensor for passive wireless blood pressure measurement. *Sensors and Actuators A: Physical*, *169*(1), 74–82. https://doi.org/10.1016/j.sna.2011.05.022

147. Jungst, T., Smolan, W., Schacht, K., Scheibel, T., & Groll, J. (2016). Strategies and Molecular Design Criteria for 3D Printable Hydrogels. *Chemical Reviews*, *116*(3), 1496–1539. https://doi.org/10.1021/acs.chemrev.5b00303

148. Wendel, B., Rietzel, D., Kühnlein, F., Feulner, R., Hülder, G., & Schmachtenberg, E. (2008). Additive Processing of Polymers. *Macromolecular Materials and Engineering*, *293*(10), 799–809. https://doi.org/10.1002/mame.200800121

149. El-Sayegh, S., Romdhane, L., & Manjikian, S. (2020). A critical review of 3D printing in construction: benefits, challenges, and risks. *Archives of Civil and Mechanical Engineering*, *20*(2), 34. https://doi.org/10.1007/s43452-020-00038-w

150. Yan, Q., Dong, H., Su, J., Han, J., Song, B., Wei, Q., & Shi, Y. (2018). A Review of 3D Printing Technology for Medical Applications. *Engineering*, *4*(5), 729–742. https://doi.org/10.1016/j.eng.2018.07.021

151. Mantihal, S., Kobun, R., & Lee, B.-B. (2020). 3D food printing of as the new way of preparing food: A review. *International Journal of Gastronomy and Food Science*, *22*, 100260. https://doi.org/10.1016/j.ijgfs.2020.100260

152. Fischer, J., & Wegener, M. (2013). Three-dimensional optical laser lithography beyond the diffraction limit. *Laser & Photonics Reviews*, *7*(1), 22–44. https://doi.org/10.1002/lpor.201100046

153. Kawata, S., Sun, H.-B., Tanaka, T., & Takada, K. (2001). Finer features for functional microdevices. *Nature*, *412*(6848), 697–698. https://doi.org/10.1038/35089130

154. Göppert-Mayer, M. (2009). Elementary processes with two quantum transitions. *Annalen der Physik*, *18*(7–8), 466–479. https://doi.org/10.1002/andp.200910358

155. Kaiser, W., & Garrett, C. G. B. (1961). Two-Photon Excitation in CaF2: Eu2+. *Physical Review Letters*, *7*(6), 229–231. https://doi.org/10.1103/PhysRevLett.7.229

156. Zhou, X., Hou, Y., & Lin, J. (2015). A review on the processing accuracy of two-photon polymerization. *AIP Advances*, *5*(3), 030701. https://doi.org/10.1063/1.4916886

157. Baldacchini, T. (2016). *Three-Dimensional Microfabrication Using Two-photon Polymerization*. Elsevier. https://doi.org/10.1016/C2014-0-01016-7

158. Maruo, S., Nakamura, O., & Kawata, S. (1997). Three-dimensional microfabrication with two-photon-absorbed photopolymerization. *Optics Letters*, *22*(2), 132. https://doi.org/10.1364/OL.22.000132

159. Park, S., Nguyen, D.-V., & Kang, L. (2021). Immobilized nanoneedle-like structures for intracellular delivery, biosensing and cellular surgery. *Nanomedicine*, *16*(4), 335–349. https://doi.org/10.2217/nnm-2020-0337

160. Kim, J. A., Wales, D. J., Thompson, A. J., & Yang, G. (2020). Fiber-Optic SERS Probes Fabricated Using Two-Photon Polymerization For Rapid Detection of Bacteria. *Advanced Optical Materials*, *8*(9), 1901934. https://doi.org/10.1002/adom.201901934

161. Li, J., Fejes, P., Lorenser, D., Quirk, B. C., Noble, P. B., Kirk, R. W., … McLaughlin, R. A. (2018). Two-photon polymerisation 3D printed freeform micro-optics for optical coherence tomography fibre probes. *Scientific Reports*, *8*(1), 14789. https://doi.org/10.1038/s41598-018-32407-0

162. Cumpston, B. H., Ananthavel, S. P., Barlow, S., Dyer, D. L., Ehrlich, J. E., Erskine, L. L., … Perry, J. W. (1999). Two-photon polymerization initiators for three-dimensional optical data storage and microfabrication. *Nature*, *398*(6722), 51–54. https://doi.org/10.1038/17989

163. Weber, K., Werdehausen, D., König, P., Thiele, S., Schmid, M., Decker, M., … Giessen, H. (2020). Tailored nanocomposites for 3D printed micro-optics. *Optical Materials Express*, *10*(10), 2345. https://doi.org/10.1364/OME.399392

164. Bunea, A., Martella, D., Nocentini, S., Parmeggiani, C., Taboryski, R., & Wiersma, D. S. (2021). Light-Powered Microrobots: Challenges and Opportunities for Hard and Soft Responsive Microswimmers. *Advanced Intelligent Systems*, *3*(4), 2000256. https://doi.org/10.1002/aisy.202000256

165. Engay, E., Bunea, A.-I., Chouliara, M., Bañas, A., & Glückstad, J. (2018). Natural convection induced by an optically fabricated and actuated microtool with a thermoplasmonic disk. *Optics Letters*, *43*(16), 3870. https://doi.org/10.1364/OL.43.003870

166. Doraiswamy, A., Ovsianikov, A., Gittard, ShaunD., Monteiro-Riviere, NancyA., Crombez, R., Montalvo, E., … Narayan, RogerJ. (2010). Fabrication of Microneedles Using Two Photon Polymerization for Transdermal Delivery of Nanomaterials. *Journal of Nanoscience and Nanotechnology*, *10*(10), 6305–6312. https://doi.org/10.1166/jnn.2010.2636

167. Bunea, A.-I., Jakobsen, M. H., Engay, E., Bañas, A. R., & Glückstad, J. (2019). Optimization of 3D-printed microstructures for investigating the properties of the mucus biobarrier. *Micro and Nano Engineering*, *2*, 41–47. https://doi.org/10.1016/j.mne.2018.12.004

168. Sabaté Rovira, D., Nielsen, H. M., Taboryski, R., & Bunea, A.-I. (2021). Additive manufacturing of polymeric scaffolds for biomimetic cell membrane engineering. *Materials & Design*, *201*, 109486. https://doi.org/10.1016/j.matdes.2021.109486

169. Narayan, R. J., Doraiswamy, A., Chrisey, D. B., & Chichkov, B. N. (2010). Medical prototyping using two photon polymerization. *Materials Today*, *13*(12), 42–48. https://doi.org/10.1016/S1369-7021(10)70223-6

170. Wu, S., Serbin, J., & Gu, M. (2006). Two-photon polymerisation for three-dimensional micro-fabrication. *Journal of Photochemistry and Photobiology A: Chemistry*, *181*(1). https://doi.org/10.1016/j.jphotochem.2006.03.004

171. Farsari, M., & Chichkov, B. N. (2009). Two-photon fabrication. *Nature Photonics*, *3*(8), 450–452. https://doi.org/10.1038/nphoton.2009.131

172. Khalil, I. S. M., Dijkslag, H. C., Abelmann, L., & Misra, S. (2014). MagnetoSperm: A microrobot that navigates using weak magnetic fields. *Applied Physics Letters*, *104*(22), 223701. https://doi.org/10.1063/1.4880035

173. Bunea, A.-I., del Castillo Iniesta, N., Droumpali, A., Wetzel, A. E., Engay, E., & Taboryski, R. (2021). Micro 3D Printing by Two-Photon Polymerization:

Configurations and Parameters for the Nanoscribe System. *Micro*, *1*(2), 164–180. https://doi.org/10.3390/micro1020013

174. Brugger, K. (1964). Thermodynamic Definition of Higher Order Elastic Coefficients. *Physical Review*, *133*(6A), A1611–A1612. https://doi.org/10.1103/PhysRev.133.A1611

175. Hruska, C. K. (n.d.). Nonlinear constants of quartz thirty years after the first nonlinear elastic tensor. In *Proceedings of 1996 IEEE International Frequency Control Symposium* (pp. 179–182). IEEE. https://doi.org/10.1109/FREQ.1996.559840

176. Thurston, R. N., McSkimin, H. J., & Andreatch, P. (1966). Third-Order Elastic Coefficients of Quartz. *Journal of Applied Physics*, *37*(1), 267–275. https://doi.org/10.1063/1.1707824

177. IRE Standards on Piezoelectric Crystals: Determination of the Elastic, Piezoelectric, and Dielectric Constants-The Electromechanical Coupling Factor, 1958. (1958). *Proceedings of the IRE*, *46*(4), 764–778. https://doi.org/10.1109/JRPROC.1958.286778

178. Bechmann, R. (1958). Elastic and Piezoelectric Constants of Alpha-Quartz. *Physical Review*, *110*(5), 1060–1061. https://doi.org/10.1103/PhysRev.110.1060

179. Ballato, A. (2001). Elastic properties of crystalline quartz . In *Handbook of Elastic Properties of Solids, Liquids, and Gases* (Vol. 2, pp. 257–279). San Diego: Academic Press.

180. Nelson, D. F. (1993). *Piezoelectric, Pyroelectric, and Related Constants*. (D. F. Nelson, Ed.) (Vol. 29b). Berlin/Heidelberg: Springer-Verlag. https://doi.org/10.1007/b44419

RESUME

Personal Details:

Name Surname : Tayyab WAQAR

Educational Details:

Education Level	Year	Program	University
Doctor of Philosophy (PhD)	2022	Mechatronics Engineering	Marmara University
Master of Science (MSc)	2015	Mechatronics Engineering	Marmara University
Bachelor of Engineering (BE)	2012	Electronics Engineering	Dawood College of Engineering and Technology

Work Experience:

Year	Company	Position
2021 – Present	Arçelik A.Ş.,	Senior Specialist Research and Development – Sensor Technologies and Mechatronics
2019 – 2021	Arçelik A.Ş.,	Specialist Research and Development – Sensor Technologies and Mechatronics
2016 – 2019	Arçelik A.Ş.,	Project Executive Research and Development – Sensor Technologies and Mechatronics
2015 – 2016	Aymaksan Ayla Makina A.Ş.	Head of Automation
2014 – 2015	Marmara University	Research Assistant

Publications:

- *"Advances in tannic acid-incorporated biomaterials: Infection treatment, regenerative medicine, cancer therapy, and biosensing",* Chemical Engineering Journal, Online Link. (Published in December 2021)
- *"Manufacturing of Microfluidic Sensors Utilizing 3D Printing Technologies: A Production System",* Journal of Nanomaterials, Online Link. (Published in August 2021)
- *"Design and Analysis Comparison of Surface Acoustic Wave-Based Sensors for Fabrication Using Additive Manufacturing",* Journal of Nanomaterials, Online Link. (Published in July 2021)
- *"Automatic decision making system with environmental and traffic data",* Mathematical Models in Engineering, Online Link. (Published in June 2021)
- *"Fabrication of Bidirectional Electrothermal Microactuator by Two-Photon Polymerization",* Current Nanoscience, Online Link (Accepted for Publication, October 2020).
- Book titled *"Autonomous Vehicle and Smart Traffic",* IntechOpen, Online Link (Published September 2020).
- *"Game Theory-Based Autonomous Vehicle Control Via Image Processing, Autonomous Vehicle and Smart Traffic",* IntechOpen, Online Link (Published in September 2020).
- "*Thermal Analysis and MLP Neural Network Based Fault Diagnosis on Worm Gears", Elsevier* Measurement (Science Direct), Online Link (Published in April 2016).
- "*Fault diagnosis on bevel gearbox with neural network and feature selection",* Elektronika IR Elektrotechnika, Online Link (Published in 3rd Quarter of 2015).
- *"Washing machine using fuzzy logic"*, Automation, Control and Intelligent Systems, Online Link (Published on 30th June, 2014).
- *"Fuzzy logic controlled automatic vacuum cleaner"*, Journal of Engineering and Technology Research, Online Link (Published in February, 2014).

Conferences:

- *"Direction-Action Research for Design, Analysis, and Fabrication of Temperature Sensor Using Microstreolitography Technique",* Online Link (Published in October 2019).
- "*ELECTRONICS 2015",* International conference (Palanga,15-17 June 2015).